Neuronal Dynamics and Brain Connectivity

Michael Breakspear[1,2] and Viktor K Jirsa[3,4]

[1] School of Psychiatry, University of New South Wales, and The Black Dog Institute, Randwick, NSW, 2031, Australia.
[2] School of Physics, University of Sydney, NSW 2006, Australia
[3] Theoretical Neuroscience Group (CNRS), UMR6152 Mouvement & Perception, 13288 Marseille, France
[4] Center for Complex Systems & Brain Sciences, Physics Department, Florida Atlantic University, Boca Raton FL33431, USA

The fluid nature of perceptual experience and the transient repetition of patterns in neurophysiological data attest to the dynamical character of neural activity. An approach to neuroscience that starts from this premise holds the potential to unite neuronal connectivity and brain activity by treating space and time in the same framework. That is the philosophy of this chapter. Our goals are threefold: Firstly, we discuss the formalism that is at the heart of all dynamical sciences, namely the *evolution equation*. Such an expression ties the temporal unfolding of a system to its physical properties and is typically a differential equation. The form of this equation depends on whether time and space are treated as continuous or discrete entities. Secondly, we aim to motivate, illustrate and provide definitions for the language of dynamical systems theory - that is, the theoretical framework that integrates analysis and geometry, hence permitting the qualitative understanding and quantitative analysis of evolution equations. To this end we provide a mini-encyclopedia of the basic terms of phase space analysis and a description of the basic bifurcations of dynamics systems. Our third aim is to provide a survey of single neuron and network models from a historical and pedagogical perspective. Here we first trace microscopic models from their birth in the 1950's showing how the neuronal firing properties can be understood as a bifurcation in the underlying phase space. Then we review the spatiotemporal network dynamics, which emerges as a function of the networks anatomical connectivity.

Introduction: Dynamics and the Brain

The firing of a neuron subsequent to an increase in synaptic input is a crucial neuronal event that is best understood from a dynamic system perspective. Whilst statistical techniques are crucial to the detection of synchrony and

change in neuroscience data, the study of dynamics uniquely permits an understanding of their causes. "Evolution" equations – which embody a system's dynamics - form the basis of all major theories in the physical sciences, from Newton's $F = ma$ to Schrödinger's wave equation and Maxwell's electromagnetic theory. There is no reason to believe that mathematical formalisms of neuronal dynamics won't eventually underpin and unify neuroscience. Indeed, over recent decades, dynamical formulations of brain activity have become sufficiently advanced to give rough outline to a "unified theory of brain dynamics". Such a theory will also inform studies of brain connectivity.

What is the origin of the brain's dynamic character? During the 20^{th} century, extraordinary progress was made in elucidating basic neurophysiological processes and their role in neural phenomena such as neuronal firing and action potential propagation. Incorporating these processes into a set of evolution equations yielded quantitatively accurate spikes and thresholds, leading to the Nobel prize for Hodgkin and Huxley. These equations are based upon the physical properties of cell membranes and the ion currents passing through transmembrane proteins. Extending this theory from a patch of cell membrane to whole neurons and thence to populations of neurons in order to predict macroscopic signals such as the electroencephalogram (EEG) is a dominant focus in this field today. Linking neuronal dynamics to theories of cognition also remains a major goal.

Dynamics has a spatial as well as a temporal character and this makes it relevant to the subject of this handbook, brain connectivity. It can be argued that all forms of information processing in neuronal systems can be understood as particular types of spatiotemporal dynamics and their bifurcations. With this in mind, our primary objective is to provide a "ground-up" overview of the dynamical approach to neuroscience. We also aim to overview some of the recent developments in this field, such as those that establish a link between statistics and dynamics and proposals that provide putative network-based cognitive mechanisms with a biophysical underpinning. Attempts to employ dynamics to unify neurophysiological phenomena are also covered. Section 4, dealing with macroscopic spatiotemporal dynamics, implicitly incorporates connectivity by way of its joint treatment of space and time.

Section 1 provides an overview of the central concept of dynamics - the "evolution equation" - and reviews the variety of forms that it can assume. In Sect. 2, we overview the mathematical concepts required to understand the behavior of such equations, with an emphasis on a geometric approach. In doing so, we also show how many of the stochastic approaches more familiar to neuroscientists are specific forms of dynamical systems when they satisfy certain stability conditions. In Sect. 3, we provide a taxonomy of key neuronal models – that is, particular forms of neuronal evolution equations, with an emphasis on small scale systems. Section 4 then focuses on large scale neuronal dynamics. We argue that there is a one-to-one relationship between modes of information processing in neuronal systems and their spatiotemporal

dynamics. Likewise, changes between such forms correspond directly with changes in the dynamics, mediated by a bifurcation or similar mechanism. The chapter concludes in Sect. 5 with some of the exciting recent developments in the field of neuronal dynamics and their putative links to other "hot topics" in neuroscience.

1 Evolution Equations: How to Make a Dynamical System

Evolution equations lie at the heart of dynamics. They state how a set of dynamical variables change in accordance with the underlying properties of the system they characterize. The most famous example of an evolution equation is Newton's "second law of mechanics" which describes the acceleration of an object as $\mathbf{F} = m\mathbf{a}$. More technically this is written as,

$$\frac{d\mathbf{v}\,(t)}{dt} = \frac{\mathbf{F}}{m}, \qquad \frac{d\mathbf{x}(t)}{dt} = \mathbf{v}\,(t) \tag{1}$$

where $\mathbf{v(t)}$ is the velocity of an object at position $\mathbf{x}(t)$. The left hand sides (LHSs) of these equations express the temporal derivative – the rate of change of a variable. The right hand sides (RHSs) link these changes to the properties of the system. The goal of calculus is to understand the resulting evolution of these variables as a function of time. In (1), it is possible to find an explicit solution for the evolution of $\mathbf{x}$ in terms of time,

$$\mathbf{x}(t) = \mathbf{x}(0) + \mathbf{v}\,(0)\,t + \frac{\mathbf{F}t^2}{2m}\,, \tag{2}$$

where $\mathbf{x}(0)$ and $\mathbf{v}(0)$ are the 'initial conditions' of $\mathbf{x}$ and $\mathbf{v}$. Equation (2) allows us to know the exact future position of an object given its current state and any applied constant force. We can see that as time increases the RHS of (2) will be dominated by the quadratic term, t^2 so that an object subject to a constant force will be increasingly rapidly displaced. In more complex systems, as encountered in neuroscience, such explicit closed form solutions generally cannot be found. Moreover, their approximations are typically so cumbersome that understanding the nature of the dynamics from such algebraic equations is not straightforward. However, one may gain a deep understanding of the nature of a system's dynamics without relying only on algebraic solutions. This can be achieved through the geometric approach to dynamical systems, outlined in Sect. 2, which unifies algebraic analysis and topology.

The essential requirements for an evolution equation are a set of evolving variables which we denote $\mathbf{Z}(\mathbf{x}, t)$ and a set of system parameters denoted $\mathbf{a}$. The former represent the current states of properties such as transmembrane potentials, neuronal firing rates, extracellular field potentials, as they vary in time t and position $\mathbf{x}$. The parameters $\mathbf{a}$ are those properties which

can be considered as static or change very slowly in comparison to the dynamical variables **Z**. Nernst potentials, conduction velocities and ion channel time constants are typical neural parameters. All of these variables are then combined with a "differential operator" – which introduces the crucial factor of change – and an algebraic expression – which determines how this change relates to the properties of the system – to form an evolution equation.

We now progress through the various forms that such equations can assume, from the simplest to the more complex. Exemplar neuronal models of each system are given in Sect. 3. Further suggested reading is provided where appropriate.

1.1 Difference Maps: Discrete Time and Discrete Space

The simplest form of determining the future state of a dynamical system from its present state is through a *difference map*,

$$\mathbf{Z}\left(t+1\right) = \mathrm{F}_{\mathbf{a}}\left[\mathbf{Z}\left(t\right)\right], \tag{3}$$

where t runs discretely as 0,1,2,... Note that the subscript **a** denotes the parameterization of F. The so-called "logistic" equation,

$$\mathrm{F}_{a}\left[Z\left(t\right)\right] = aZ(1-Z), \tag{4}$$

is a very well-known one-dimensional (scalar) example of a difference equation. The evolution of this relatively simple (quadratic) nonlinear equation is illustrated in Fig. 1.

The logistic map, and other simple algebraic forms, has been used extensively to elucidate basic, generic properties of nonlinear dynamics (Collet & Eckmann 1980, Cvitanovic 1984). They can exhibit a rich complexity even when the algebraic equations are simple as in (4). Examples of their use include elucidating the fundamental principles of chaotic dynamics (Guckenheimer 1987) and the transition from regular to chaotic motions (Feigenbaum

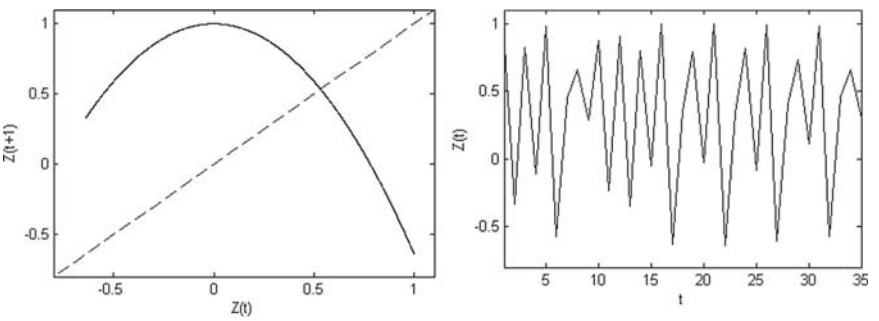

Fig. 1. (**a**) Logistic equation (4) with $a = 1.64$. (**b**) Resulting chaotic time series. Maps of this type have been used to study the basic properties of nonlinear systems. They have a less extensive role in modeling neural systems

1987). These concepts are discussed and illustrated in Sect. 2, below. An excellent introduction to this fascinating field is given by Baker & Gollub (1990).

The spatiotemporal properties of nonlinear dynamics can also be studied within this framework, through the use of *coupled difference maps*,

$$\mathbf{Z}\left(x_i, t+1\right) = \mathrm{F}_{\mathbf{a}}\left(\mathbf{Z}\left(x_i, t\right), \sum_{j \neq i} \mathrm{H}_c\left[\mathbf{Z}\left(x_j, t\right)\right]\right) \tag{5}$$

where x_i denotes the spatial position of the i-th subsystem. The "coupling function" H_c introduces the activity from all other nodes into the dynamics of this node. The subscript c denotes the strength of the coupling influence and is traditionally normalized so that $0 \leq c \leq 1$. Hence, if F embodies local neural dynamics, H incorporates the spatial characteristics of synaptic connectivity. Just as autonomous difference maps can be used to elucidate basic dynamical principles, coupled difference maps permit an understanding of the fundamentals of dynamic synchronization (Maistrenko et al. 1998). Often the influence of the local versus global dynamics can be linearly partitioned as,

$$\mathbf{Z}\left(x_i, t+1\right) = \mathrm{F}_{\mathbf{a}}\left[\mathbf{Z}\left(x_i, t\right)\right] + \sum_{j \neq i} \mathrm{H}_c\left[\mathbf{Z}\left(x_j, t\right)\right]. \tag{6}$$

A fascinating, early example of a coupled difference-map neural model is that of McCulloch & Pitts (1943) which we discuss in Sect. 3. However, because of the discrete nature of time in difference maps, and the fact that their study has been characterized by using very basic algebraic expressions, they rarely figure in biophysical models of neural systems. On the other hand, they have been used extensively to study the basic properties of high dimensional nonlinear dynamics (Kaneko 1997), including the onset of synchronization amongst two or more subsystems (Ashwin et al 1997). Put another way, they are mathematically pleasing because they permit an analytic understanding of the universal principles of dynamics and synchronization, but limited in their value to neuroscientists because their simplicity prohibits one from identifying the relative contribution of particular physiological processes to specific dynamical behaviors.

1.2 Ordinary Differential Equations: Continuous Time and Discrete Space

One obvious step towards physiological realism is to make time continuous! This can be achieved by exploring neural systems, whose evolution is governed by an ordinary differential equation (ODE),

$$\frac{d\mathbf{Z}\left(t\right)}{dt} = \mathrm{F}_{\mathbf{a}}\left[\mathbf{Z}\left(t\right)\right]. \tag{7}$$

where as above $\mathbf{Z}(t)$ is a set of dynamical variables. This is the form of equation for most traditional neuronal models such as the Hodgkin Huxley

model in which case $\boldsymbol{Z}_1 = V$ is the transmembrane potential and F takes the form,

$$\mathrm{F}_{\mathbf{a}}\left[V\left(t\right)\right] = \sum_{ion} f_{ion}\left[V\left(t\right)\right] + I. \tag{8}$$

The summation on the RHS is taken over all ion channels. For each ion species

$$\frac{df_{ion}\left(t\right)}{dt} = g_{ion}\left[V\left(t\right)\right] \tag{9}$$

represents the dynamics of the local voltage-dependent channel currents for each ion species. I represents synaptic currents which flow through ligand-gated channels or via an experimentally introduced electrode. As with difference equations, spatiotemporal dynamics are achieved by employing a coupling function H_c to introduce interdependence between systems,

$$\frac{d\mathbf{Z}\left(x_i,t\right)}{dt} = F_{\mathbf{a}}\left(\mathbf{Z}\left(x_i,t\right), \sum_{j\neq i} \mathrm{H}_c\left[\mathbf{Z}\left(x_j,t\right)\right]\right). \tag{10}$$

Hence, if (8) models the dynamics of a single neural system, (10) adds the interaction between two or more systems, creating a dynamic neural network. The ensemble is spatially discrete with a finite number N of subsystems so that the subscript indices $i, j = 1, 2, \ldots, N$. As with coupled difference equations, it is often possible to bipartition the influence of the local and distant terms in (10) as

$$\frac{d\mathbf{Z}\left(x_i,t\right)}{dt} = F_{\mathbf{a}}\left(\mathbf{Z}\left(x_i,t\right)\right) + \sum_{j\neq i} \mathrm{H}_c\left[\mathbf{Z}\left(x_j,t\right)\right]. \tag{11}$$

Such is the case when local recurrent axons and long-range afferents each project onto separate classes of neurons. In this case the long-range afferents are modeled as acting, through ligand-gated ion channels, via the synaptic currents. Hence,

$$\frac{d\mathbf{Z}\left(x_i,t\right)}{dt} = \sum_{ion} f_{ion}\left[\mathbf{Z}\left(x_i,t\right)\right] + I\left(x_i,t\right), \tag{12}$$

where the induced synaptic currents,

$$I\left(x_i,t\right) = \sum_{j} \mathrm{H}_c\left[\mathbf{Z}\left(x_j, t-\boldsymbol{\tau}_j\right)\right] + I_{external}, \tag{13}$$

introduce the afferent inputs from other systems $\mathbf{Z}(x_j,t)$ that arrive after a time delay τ_j - permitting finite speed axonal conduction. Because space is discrete, the time delays are also discretely distributed. Differential equations with time delays are treated thoroughly in the Chapter by Campbell. We only introduce them here because they are important in the conceptual transition from discrete to continuous space to which we now turn. A review of neuronal synchrony as modeled by coupled ODE's is provided by Breakspear (2004).

1.3 Integrodifferential Equations: Continuous Time and Continuous Space

In the case where we wish to model the inputs to region x_i arising from a continuously distributed neuronal ensemble, we integrate the afferent induced currents (13) continuously over space,

$$I\left(x_i,t\right)=\int\limits_{\Omega}\int\limits_{-\infty}^{t}h\left(\mathbf{x}-\mathbf{x}'\right)\mathrm{H}\left[\mathbf{Z}\left(\mathbf{x}-\mathbf{x}',t-t'\right)\right]dt'd\mathbf{x}', \tag{14}$$

where the spatial integration d$\mathbf{x}$' is taken over the spatial domain Ω of the neural system. Note that this also requires that we integrate over the (now) continuously distributed time delays, t'. We have also partitioned the coupling function into two parts, H and h. H determines which variables from any given system enter into the inter-system coupling, and how they do so. Typically H itself has two components, an "activation" function that converts local membrane potentials of the distant systems into firing rates ρ - which then propagate outwards - and synaptic kernels η which model how these propagating action potentials influence post-synaptic potentials as they arrive,

$$\mathrm{H}\left[\mathbf{Z}\left(\mathbf{x},t\right)\right]=\eta\left(t\right)\rho\left(\mathbf{Z}\left(\mathbf{x},t\right)\right) \tag{15}$$

Specific forms of η and ρ are provided in Sect. 4. The coupling function h captures the spatial dependency of the strength of the afferent inputs. This function is also known as the 'synaptic footprint' (Coombes 2003) because it reflects the nature and density of synaptic connections as they change with the distance from their origin. Substituting the synaptic inputs (14) into the differential (12) and collapsing all local contributions into

$$N\left[\mathbf{Z}\left(\mathbf{x},t\right)\right]=\sum_{ion}f_{ion}\left[\mathbf{Z}\left(\mathbf{x},t\right)\right] \tag{16}$$

we obtain

$$\frac{d\mathbf{Z}\left(\mathbf{x},t\right)}{dt}=N(\mathbf{Z}\left(\mathbf{x},t\right))+\int\limits_{\Omega}\int\limits_{-\infty}^{t}h\left(\mathbf{x}-\mathbf{x}'\right)\mathrm{H}\left(\mathbf{Z}\left(\mathbf{x}-\mathbf{x}',t-t'\right)\right)dt'd\mathbf{x}', \tag{17}$$

an integrodifferential equation. It may be considered a general form of a neural mass model because the exact nature of the synaptic "footprint", the activation function and the synaptic kernels remain unspecified. For example within this framework, it would be possible to use the precise form of the lateral inhibition that has been shown to allow sensory networks to be inherently tuned to particular spatial frequencies (Ratliff et al. 1969).

1.4 Partial Differential Equations: Continuous Time and Continuous Space but Constrained Connectivity

In some contexts, it may be preferable to express (17) with spatial and temporal derivatives only - rather than a combination of temporal derivatives with spatial and temporal integrations. Such differential representation is useful if the connectivity function h is sufficiently simple, smooth and translationally invariant, because then only a few spatial derivatives are needed to capture the connectivity. For example, given appropriate forms of h and H (see sect. 4) (17) can be rewritten as a partial differential equation of the form,

$$\frac{\partial^2 \mathbf{Z}(\mathbf{x},t)}{\partial^2 t} + a\frac{\partial \mathbf{Z}(\mathbf{x},t)}{\partial t} + b\frac{\partial^2 \mathbf{Z}(\mathbf{x},t)}{\partial^2 x} + c\mathbf{Z}(\mathbf{x},t) = (d + \frac{\partial}{\partial t})\rho(\mathbf{Z}(\mathbf{x},t)) \quad (18)$$

The coefficients $a,\ b,\ c$ and d depend on system parameters such as conduction velocities and the synaptic footprint parameter σ. Such an equation, expressing the evolution of neuronal systems, continuously in space and time, but with specific types of connectivity was first derived for macroscopic neuronal dynamics by Jirsa and Haken (1996, 1997) and Robinson et al. (1997). Pioneering work that led to this formulation started as early as the 1970s (Wilson 1973, Wilson & Cowan 1973, Nunez 1974, van Rotterdam et al. 1982). Comparing (11) and (18) we see that in the former, spatial coupling is introduced explicitly through the second term on the right hand side. In the latter, space enters the temporal dynamics through the (second order) spatial derivative on the left hand side. However, under certain conditions these two approaches can be equivalent.

1.5 Stochastic Differential Equations

All of the equations above capture the dynamical evolution of each of the values $\mathbf{Z}$ of the system of interest. In the case of a microscopic system, these variables may include transmembrane potential and ion channel conductance of a small patch of cell membrane. Evolution equations, such as (11) and (18) may also describe neural systems in the mesoscopic (<mm) and even macroscopic (∼cm) scales. In such cases, the variables of interest represent mean values averaged over the appropriate scales. Such equations are hence known as mean field approximations. Before proceeding further, it is worth describing evolution equations which capture the dynamics for the entire probability distributions $p(\mathbf{x},t)$ rather than just the mean. Such models allow for stochastic inputs to a system which nonetheless obeys deterministic rules. They take the form,

$$\frac{\partial p(\mathbf{x},t)}{\partial t} = \frac{\partial\left((f+s)\,p(\mathbf{x},t)\right)}{\partial x} + \frac{w^2}{2}\frac{\partial^2 p}{\partial x^2} \quad (19)$$

where s represents the (stochastic) inputs to the system and f is the form of the deterministic dynamics. As described in Harrison et al. (2005), the first

term of the RHS describes the evolution of the probability distribution under the influence of the inputs s and the nature of the physiological system f. The second term describes the tendency of the distribution to disperse under the influence of the stochastic elements at rate w.

Whereas (11) and (18) are mean field equations, (19) is an example of a broader class of "neural field" equations, capturing the evolution of the entire probability distribution. There are a number of intriguing reasons to generalize neural evolution equations from mean field formulations to capture the evolution of the entire distributions. For example, consider two neural populations with the same mean membrane potentials, but where the second population has a larger variance. If the mean potential is below the threshold for firing, this difference in variance will imply that a greater proportion of neurons in the second population will be supra-threshold and hence firing (Fig. 2). These neurons, through local feedback, will in turn have a greater effect on the local mean membrane potential, driving it upwards or downwards – depending on whether the local feedback is excitatory or inhibitory. Put alternatively, modeling the entire distribution rather than just the mean permits the higher order moments of the neural states to interact (Harrison et al. 2005).

Solutions to (19) are possible only in very restricted cases. The development of numerical techniques – required to gain important insights into the dynamics – is a very active area of research. One important method in this vein relies upon a "modal decomposition", whereby the entire distribution is truncated to a few low order modes. The very restricted case, reducing such an equation to the first moment – the mean – returns us to the mean

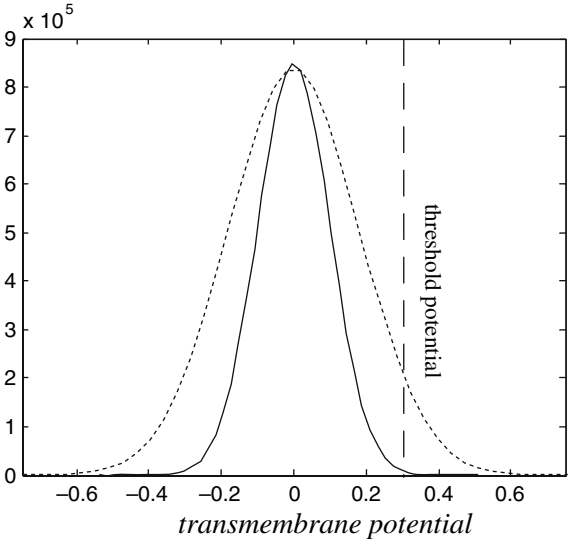

Fig. 2. Two different distributions of neural membrane potentials, with the same mean states, will in general have different mean firing rates (arbitrary units)

field formulations discussed above. In situations where higher order moments of the distribution (variance, kurtosis etc) are retained, the possibility exists for deep, but tractable representations of complex neuronal dynamics. Hence interactions between stochastic and deterministic processes, as embodied in (19) can be formally studied.

2 The Geometry of Dynamics: A Mini-Encyclopedia of Terms

In this section, we step back from a consideration of the forms that evolution equations can take and overview the crucial geometrical means of understanding them.

2.1 Basic Dynamical Concepts

As mentioned in the Introduction, nonlinear differential equations can be notoriously intractable with regards to exact analytic solutions. However, a thorough understanding of their dynamics is very often possible by combining analysis and geometry. In this Section, we provide the central defining terms through the exploration of some simple dynamical systems. In interests of brevity we have sought to explain the intuitive meaning of the terms, keeping technical definitions to a minimum. Most of these terms are given more formal definitions in standard dynamical systems textbooks (e.g. Strogatz 1994). Illustrated examples of all terms follow in subsequent sections.

For any study of geometry, we require a space in which to embed our objects of study. For evolution equations, a ***manifold*** fulfills this purpose. Put simply, a manifold is a space which can be locally stretched or deformed into a Euclidean space whilst having a variety of global shapes. Hence the local structure sustains the intuitive meaning of terms such as a ***neighbourhood*** (a ball of small radius) which are crucial for issues requiring a "distance", well defined for Euclidean space. The global structure of a manifold, on the other hand, can be quite complicated, and may be 'bounded' (like the unit interval) or 'unbounded' (like the Euclidean plane), 'simply connected' (like a sphere) or not simply connected (like a torus). A ***differentiable manifold*** has the additional properties required to support differentiation. The planar surface, a torus and a sphere are differentiable manifolds. Although the properties of these spaces may seem trivial, a formal definition of a differentiable manifold must be able to support quite general dynamical systems. For example, the manifold of a partial differential equation has infinite dimension!

A ***phase space*** is a differentiable manifold whose axes are spanned by the dynamical variables $\mathbf{Z} = \{Z_1, Z_2, Z_3, \dots\}$ of an evolution equation. The ***topology*** ("shape") of the phase space is chosen to match the properties of these variables. For example, the plane (R×R) is a suitable phase space for a system with two membrane potentials. For a system where the two variables

are phases varying between 0 and 2π, the torus $(S \times S)$ is preferable because of the periodic nature of the boundaries.

We can think of a point in phase space as the instantaneous state $\mathbf{Z}(t)$ of our system. If we substitute this state into our evolution equation, we would get the instantaneous rate of change of the system $d\mathbf{Z}(t)/\mathrm{d}t$ when in that state. This defines a ***tangent vector*** in the phase space, telling us how the system will evolve into its next state $\mathbf{Z}(t')$. This critical step – of linking dynamics to geometry – is captured by the ***vector field***, a directed flow through a phase space which embodies the evolution equation. More technically, a vector field assigns a vector to every point in phase space which is precisely the solution of the evolution equation at that point. Hence these vectors capture both the rate and direction of change of the system. For example, the vector field corresponding to the trivial one-dimensional equation $\mathrm{d}x/\mathrm{d}t = -x$ is just the set of all vectors of length x pointing towards the origin. The vector field at $x = 1$ is a vector of length 1 directed towards the origin.

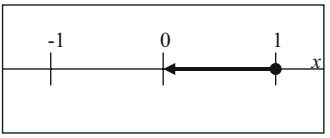

In this way the algebra of the evolution equations and the analysis methods of geometry are linked (Vector fields are often *represented* as arrows overlaid on the phase space but more technically they are defined on a related space called the ***tangent bundle***). An ***orbit*** or ***trajectory*** is a connected path through phase space which is always tangent to the vector field. Hence an orbit traces the time-dependent solution to a dynamical system through a succession of instantaneous states. It captures the manner in which a system will change according to the evolution equation. The starting point of such an orbit is called its ***initial condition***. Examples are given in Fig. 3.

$$\frac{dz_1}{dt} = z_2 \,, \qquad \frac{dz_2}{dt} = \mu\left(1 - z_1^2\right) z_2 - z_1 \,. \tag{20}$$

A time series of this system for $\mu = 2$, showing the periodic nature of the oscillations, is given in Fig. 4(a). A single orbit, commencing with an initial condition in close proximity to the origin is shown in the planar phase space spanned by z_1 and z_2 in Fig. 4(b). It can be seen that this orbit diverges rapidly away from the origin and towards a closed loop in phase space, corresponding to the appearance of periodic oscillations in the time series. The appearance of periodic oscillations in the system motivates us to consider an alternative phase space representation, achieved by a change of coordinates to amplitude A and phase θ,

$$A = \sqrt{z_1^2 + z_2^2} \,, \qquad \phi = \arctan\left({}^{z_2}\!/_{z_1}\right). \tag{21}$$

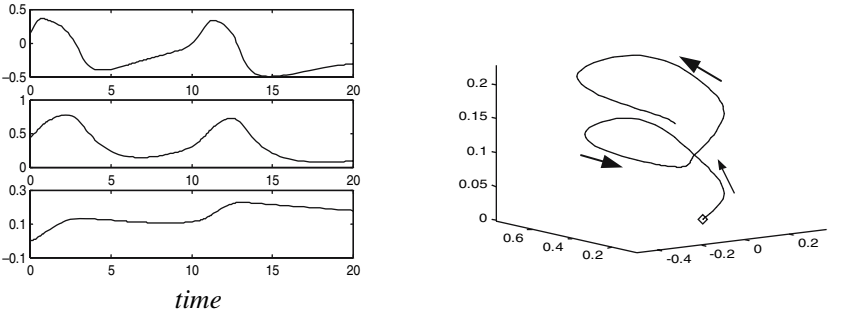

Fig. 3. Example of a time series (left hand panel) of three variables $\mathbf{Z} = \{Z_1, Z_2, Z_3, \dots\}$ of a dynamical system briefly evolving along an orbit in phase space (right hand panel). The diamond represents the initial condition and the arrows represent tangent vectors in phase space

Such a cylindrical manifold, whose periodic boundary conditions embody the nature of the oscillatory dynamics, is shown in Fig. 4c. The convergence of the orbits shown in panels (b) and (c) onto the closed loop, on which they then remain, motivates the concept of an ***invariant set*** of the dynamics. Intuitively, this is simply a set of points (e.g. single point, closed loop, etc.) in which orbits remain once they enter. More formally if $\boldsymbol{F}$ represents the flow of a dynamical system then an invariant set $\boldsymbol{A}$ satisfies $\boldsymbol{F}(\boldsymbol{A}) \subseteq \boldsymbol{A}$. The Van der Pol system in Fig. 4 has two invariant sets, one at the origin and the closed loop as shown. A variety of other orbits, from distinct initial conditions, are shown in panel (d). In each case, the orbits approach the limit cycle.

This simple observation motivates the crucial concept of an ***attractor***, a bounded (i.e. finite) invariant set which is approached by the orbits from a "large set" of initial conditions. Traditionally, a large set implied an "open neighborhood" of the attractor. More recently the concept of an attractor has been generalized to mean any set with a non-zero probability measure (Milnor 1985) meaning that there is a (possibly very small but still non-zero) chance that an orbit from a randomly chosen initial condition will flow onto the attractor. On the other hand, there may be initial conditions arbitrarily close to the attractor that nonetheless flow elsewhere. This distinction is important in the setting of synchronization (Ashwin & Terry 2000) and we explore it further below.

We have hence seen ***fixed point*** and ***limit cycle*** attractors. A ***chaotic attractor*** has already been illustrated for the logistic equation in Fig. 1. In comparison to a limit cycle which endlessly repeats its prior states, a chaotic attractor *never* repeats a state although is nonetheless bounded and invariant. More formally, a chaotic attractor exhibits ***sensitive dependence to initial conditions*** – that is any two orbits, no matter how close initially - diverge at an exponential rate. This rate of divergence is captured by the largest ***characteristic exponent***, which is positive for a chaotic attractor. In contrast,

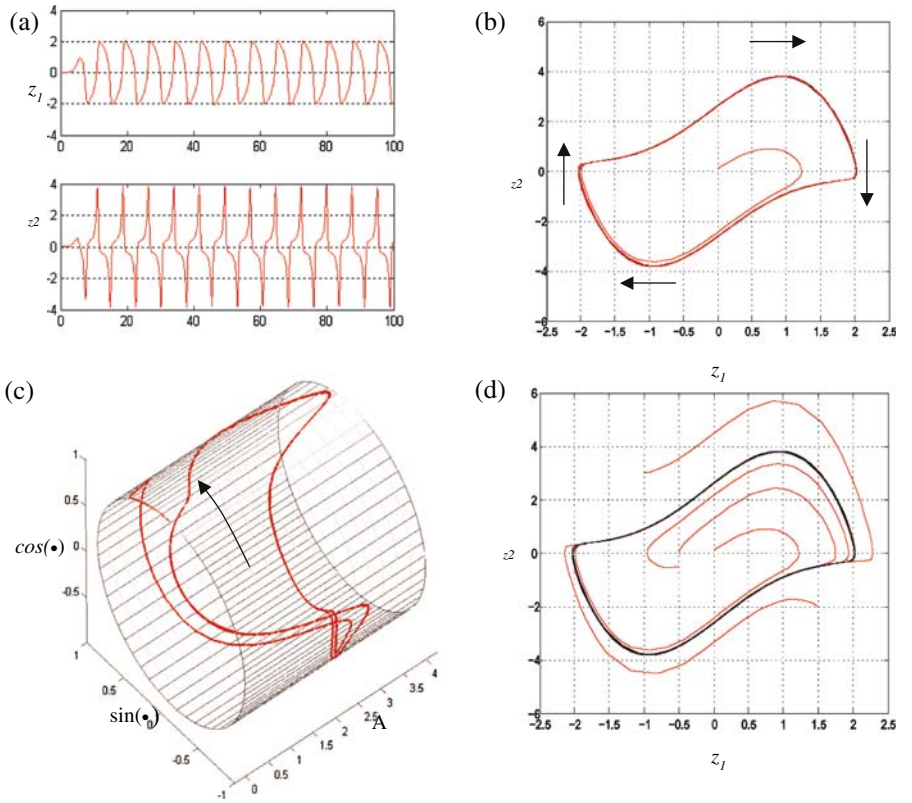

Fig. 4. Van der Pol oscillator for $\mu = 2$. (**a**) Time series. (**b**) Phase space portrait representation of a single orbit and its approach toward a limit cycle attractor. Arrows show representative vector field. (**c**) Representation of the same orbit on a cylindrical manifold spanned by the polar coordinates A(t) and θ(t). (**d**) A set of distinct initial conditions flowing toward the limit cycle attractor (black)

two such points will stay forever close if on or near a limit cycle attractor (the largest characteristic exponent is zero). Two such points in the vicinity of a fixed point attractor will invariably get closer (the largest characteristic exponent is negative). A chaotic attractor is also ***topologically mixing*** – i.e. any given open set covering any region of the attractor will eventually overlap with any other region. The unceasing divergence of nearby orbits and the eventual mixing of regions combine to enable a chaotic attractor to be both unstable and bounded. We revisit chaos in the setting of specific neuronal models in Sect. 3.

An attractor's ***basin of attraction*** is the set of all initial conditions which have the attractor as their future state. In the present case, the basin of attraction for the loop is the entire plane, except for the origin. The ***inset*** of an attractor is that part of the basin of attraction with the strongest (principle)

direction of attraction. A ***repellor*** is an invariant set that is the past state of a large set of points, its ***basin of repulsion***. The ***outset*** of a repellor is the subspace of this basin which diverges most quickly. In the present case, the origin is a repellor and its basin of repulsion is all the points within the loop.

If time was reversed in (20), the origin would become an attractor and points within the loop would be its basin of attractions. Points outside the limit cycle would diverge towards infinity. Hence the loop would be an example of a ***basin boundary*** or ***seperatrix***. Basin boundaries can be repellers (as in the case here) or saddles which have an inset and an outset. A trivial example of a saddle is the origin in the system,

$$\frac{dz_1}{dt} = a_1 z_1 + b_1 \qquad \frac{dz_2}{dt} = a_2 z_2 + b_2 \tag{22}$$

where, for $a_1 = 1,\ a_2 = -1$ and $b_1 = b_2 = 0$ the z_1-axis is the inset and the z_2-axis is the outset (Fig. 5).

Occasionally, the outset from a repellor becomes the inset of an attractor. Such an entity, linking two fixed points, is called a ***heterocline***. For a saddle, it is possible that the outset becomes the inset (due to curvature away from the saddle point). If so, it is called a ***homocline***.

Two final concepts are required before we move onto more complex matters. An attractor possesses ***structural stability*** if it is insensitive to a small change in the nature of the vector field, corresponding to a small change in the evolution equation. "Insensitivity" here denotes that there exists a smooth mapping between the perturbed attractor and the original attractor. When such a mapping exists we say the two (original and perturbed) attractors are ***topologically conjugate***. The saddle point in Fig. 5 is structurally stable following changes in either the parameters a (under a stretching and/or contraction) and/or the parameters b (under a translation). Similarly the Van der Pol attractor in Fig. 4 is structurally stable since small changes to any of the parameters results in another (topologically conjugate) limit cycle attractor.

The ***nullclines*** of a dynamical system are the curves in phase space, for which one derivative in the evolution equation is equal to zero, and hence correspond to the regimes in phase space with zero flow in a particular direction.

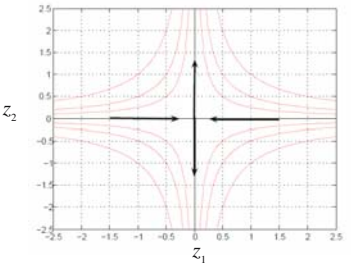

Fig. 5. Saddle point and orbits of (22)

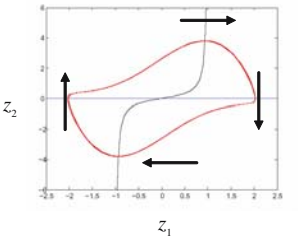

Fig. 6. Nullclines of the Van der Pol system. Arrows show direction of the vector field across the nullclines. The fixed point lies at the intersection of the two mullclines (in blue and black). The trajectory is shown in red

The two nullclines to the Van der Pol equation (20) are depicted in Fig. 6. The blue line shows the nullcline for zero flow in the z_1 direction and the black shows the curve for z_2. The limit cycle trajectory satisfies these conditions as it crosses the respective curves – that is, the $\mathrm{d}z_1/\mathrm{d}t = 0$ when the attractor (red curve) crosses the blue nullcline. By definition, any crossing of two nullclines corresponds to the existence and location of a fixed point since $\mathrm{d}z_1/\mathrm{d}t = \mathrm{d}z_2/\mathrm{d}t = 0$.

The nullclines form the "skeleton" of the phase space and, as we explore below, their intersections are vital to the existence and nature of most attractors, not just fixed points.

2.2 Bifurcations and Complex Dynamics

The preceding discussion captures the nature of phase space dynamics and its relationship to the evolution equations for a given set of parameter values (i.e. when the vector field is kept constant). An intriguing and important field of study concerns what happens to the attractors and basin boundaries following a change to the system's parameters and hence to the vector field. From above it follows that if all the attractors are structurally stable, then the effect of such a change can be considered trivial since the dynamics will remain qualitatively similar (and typically also quantitatively similar). However, in the case when this is not so, sudden and dramatic changes in the dynamics, denoted ***bifurcations***, occur. Examples abound in neuroscience, such as the generation of an action potential, the onset of bursting (Izhikevich 2005) and even the onset (Robinson et al. 2002, Lopes da Silva et al. 2003, Breakspear et al. 2006) and temporal progression (Rodriguez et al. 2006) of an epileptic seizure.

An important means of understanding the nature of a system's bifurcations is through the study of its ***bifurcation diagram***. This is produced by smoothly varying one parameter over some range of interest whilst keeping all other parameters fixed. Hence the vector field is smoothly changed in one dimension of parameter space. At each parameter value, the system is integrated and, after passage of an initial transient – allowing for the system to

evolve towards its attractor(s) – the asymptotic time series is captured. From this time series, the values of all local minima and maxima are stored. For a fixed point there will exist only one such value. For a simple (period-1) limit cycle there will exist two such points and for a period-2 oscillator, four such points – two maxima and two minima. For a chaotic oscillator, such points will be distributed ***densely*** ("almost everywhere") over one of more segments. The bifurcation diagram is the plot of these local maxima and minima against the respective parameter value. Figure 7 shows the bifurcation diagram of the logistic (4).

It is crucial to note that in most nonlinear systems, two or more attractors may co-exist for some parameter values, facilitating ***bistability*** or even ***multistability***. Each attractor will have basins, each separated by basin boundaries. In such cases, it is important that all such attractors are located when plotting a bifurcation diagram.

Bifurcations can be divided into local and global, as outlined below. Before doing so, it is important to introduce a second notion of stability. Structural stability concerns the robustness of invariant sets – attractors, repellors, saddles - to changes in the underlying vector field. In contrast ***asymptotic stability*** deals with the situation where the instantaneous state of the system is perturbed through addition of a small transient noise term (but the vector field is kept constant). An attractor is called asymptotically stable whenever the system returns towards the attractor following any such (small)

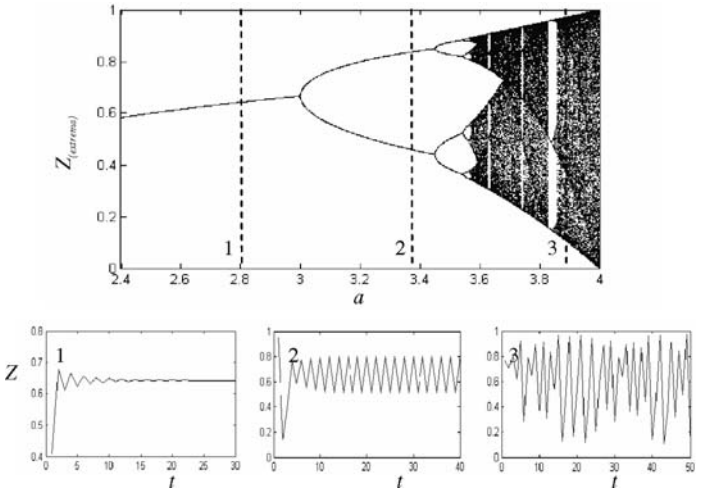

Fig. 7. Bifurcation diagram of the logistic equation (**4**). Top panel shows the local minima and maxima of the asymptotic time series against the parameter a. Lower three panels show representative time series (including the initial transient) with (**1**) fixed point, (**2**) limit cycle and (**3**) chaotic attractors. Note the "periodic windows" within the chaotic regime of the bifurcation diagram

noisy perturbation. A ***local bifurcation*** occurs whenever an attractor loses *asymptotic* stability whereas a ***global bifurcation*** corresponds to the loss of *structural* stability. These are also called *subtle* and *catastrophic* bifurcations (Abraham & Shaw 1988) because in the latter case the impact on the dynamics is typically more immediately discernable. We now explore such bifurcations in further detail.

Local Bifurcations

Local bifurcations concern the asymptotic stability of fixed point and other attractors. Consider the system governed by,

$$\frac{d\mathbf{Z}}{dt} = \mathbf{AZ} + \mathbf{B}, \tag{23}$$

where $\mathbf{A}$ is a matrix and $\mathbf{B}$ a vector. This is the matrix form of (22). Solutions in the case where $\mathbf{B}$ is zero are of the form

$$\mathbf{Z}(t) = \mathbf{Z}(0)\, e^{t\mathbf{A}}. \tag{24}$$

Hence the origin is a fixed point and the eigenvalues Λ of $\mathbf{A}$ determine the nature of the neighboring flow. Solutions in the case $\mathbf{B} \neq 0$ are essentially the same after a suitable translation of the axes. The eigenvalues $\Lambda = \{\lambda_1,\ \lambda_2\}$ determine five possible types of fixed point systems (Fig. 8).

Figure 8(a) shows a typical flow when both eigenvalues are real and either both positive or both negative. Orbits diverge from ($\lambda_1 > 0,\ \lambda_2 > 0$) or converge to ($\lambda_1 < 0,\ \lambda_2 < 0$) the origin. In the former case, the fixed point is called a ***source*** and in the latter, a ***sink*** or ***node***. We have already met the case (Fig. 8b) where the eigenvalues are real and opposite in sign ($\lambda_1 > 0,\ \lambda_2 < 0$) for the ***saddle point*** discussed above with regards to basin boundaries. When the eigenvalues are complex, they occur as complex conjugate pairs. The imaginary component endows the time series with an oscillatory component evident as spiraling orbits (Fig. 8c). When the real part of each eigenvalue is negative, these oscillations are damped and the fixed point is a ***spiral inset***. Otherwise it is a ***spiral outset***.

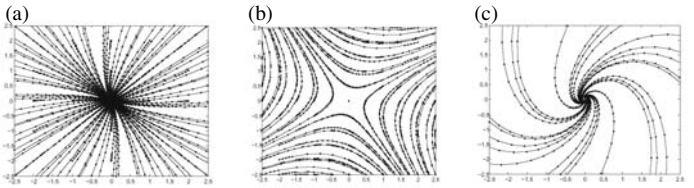

Fig. 8. Orbits for fixed points of the linear system (26). (**a**) Source or sink, (**b**) saddle, and (**c**) Spiral inset or outset

Whilst (26) is a simple linear system, the ***Hartman-Grobman theorem*** states that, for a very general class[5] of nonlinear systems $\mathbf{F}_{\mathrm{a}}$, the flow within the neighborhood of a fixed point can be approximated by a suitable linear system with the form of (23). Hence these fixed points – and their stability – play an important role in many dynamical systems.

Note that the eigenvalues of $\mathbf{A}$ determine the divergence or convergence of nearby orbits. These are hence the "characteristic exponents" referred to in Sect. 2.1. In the setting of fixed points these are simply referred to as the eigenvalues of $\mathbf{A}$. They are often called ***Floquet exponents*** in the vicinity of a limit cycle and ***Lyapunov exponents*** for a chaotic attractor. Following Eckmann and Ruelle (1984), we will simply refer to them as characteristic exponents, whatever the nature of the invariant set to which they refer.

Local bifurcations hence deal with the zero crossings of the characteristic exponents of attractors. The underlying set (typically) remains invariant, but loses its asymptotic stability. Just as a zero crossing can transform a fixed point from an attracting node into a saddle, the same also applies for both limit cycles and chaotic attractors. We now briefly discuss some of the canonical local bifurcations. In sect. 3 we will see how they relate to fundamental neuronal events such as firing and bursting.

Canonical Local Bifurcations

Pitchfork bifurcations occur when a single fixed point changes its (asymptotic) stability whilst also splitting off extra fixed points. In a ***supercritical pitchfork bifurcation*** a single stable fixed point attractor loses its stability as a parameter crosses its threshold and two new stable fixed points appear (Fig. 9a). The evolution equation,

$$\frac{dz}{dt} = z\left(a - z^2\right), \tag{25}$$

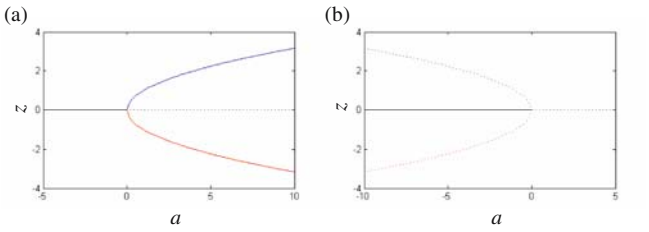

Fig. 9. Pitchfork bifurcation diagram (**a**) Supercriticial, and (**b**) subcritical. Solid line denotes fixed point attractor. Dashed lines denote fixed point repellors

[5] As long as the derivative of $\mathbf{F}_{\mathrm{a}}$ at the fixed point is not zero – i.e. the fixed point is *hyperbolic*.

yields this type of bifurcation at $a = 0$. Note that for $a < 0$, we have $dz/dt < 0$ when $z > 0$ and $dz/dt > 0$ when $z < 0$. Hence all initial conditions lead to the fixed point $z = 0$. Similar calculations show that when A crosses zero ($a > 0$) the origin becomes a source and fixed point attractors exist as $\pm\sqrt{a}$.

On the other hand the equation,

$$\frac{dz}{dt} = z\left(a + z^2\right), \tag{26}$$

yields a ***subcritical pitchfork bifurcation***. In this case, the fixed point attractors at $z = 0$ also loses its stability as A crosses zero from below. However, two fixed point repellors exist at $\pm\sqrt{-a}$ when $a < 0$ (Fig. 9b). Looking at the situation alternatively, one could say that the fixed point attractor at $z = 0$ loses its stability when two fixed point repellors collide with it at $a = 0$. However, in both cases, the fixed point remains an invariant of the system (i.e. $dz/dt = 0$) for all a.

In a ***transcritical bifurcation***, there are two equilibrium points which collide and exchange their stability at the bifurcation point. For example, the evolution equation,

$$\frac{dz}{dt} = z\left(a - z\right), \tag{27}$$

has two equilibrium points, the origin $x = 0$ and $x = a$. When $a < 0$, the origin is an attractor but becomes a repellor as a crosses zero (Fig 10).

A ***Hopf bifurcation*** (Fig. 11) is much like a pitchfork bifurcation with the exception that it involves a limit cycle attractor. Hopf bifurcations play an important role in neuronal models as they describe the onset of both subthreshold membrane oscillations and cell firing. Consider the equation,

$$\frac{dz}{dt} = z\left(a + b\left|z\right|^2\right), \tag{28}$$

where a is the bifurcation parameter and both z and b are complex numbers. When the real part of b is negative then the system exhibits a ***supercritical Hopf bifurcation*** (Fig. 11a,c–f). For $a < 0$ there exists a single stable fixed point attractor (a spiral inset). When $a > 0$ this fixed point is an unstable spiral outset and there also exists a stable limit cycle.

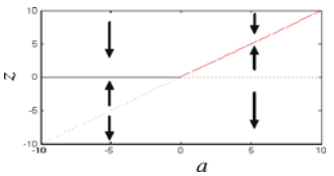

Fig. 10. Transcritical bifurcation. Solid line denotes fixed point attractor. Dashed lines denote fixed point repellors. Arrows show representative vector field

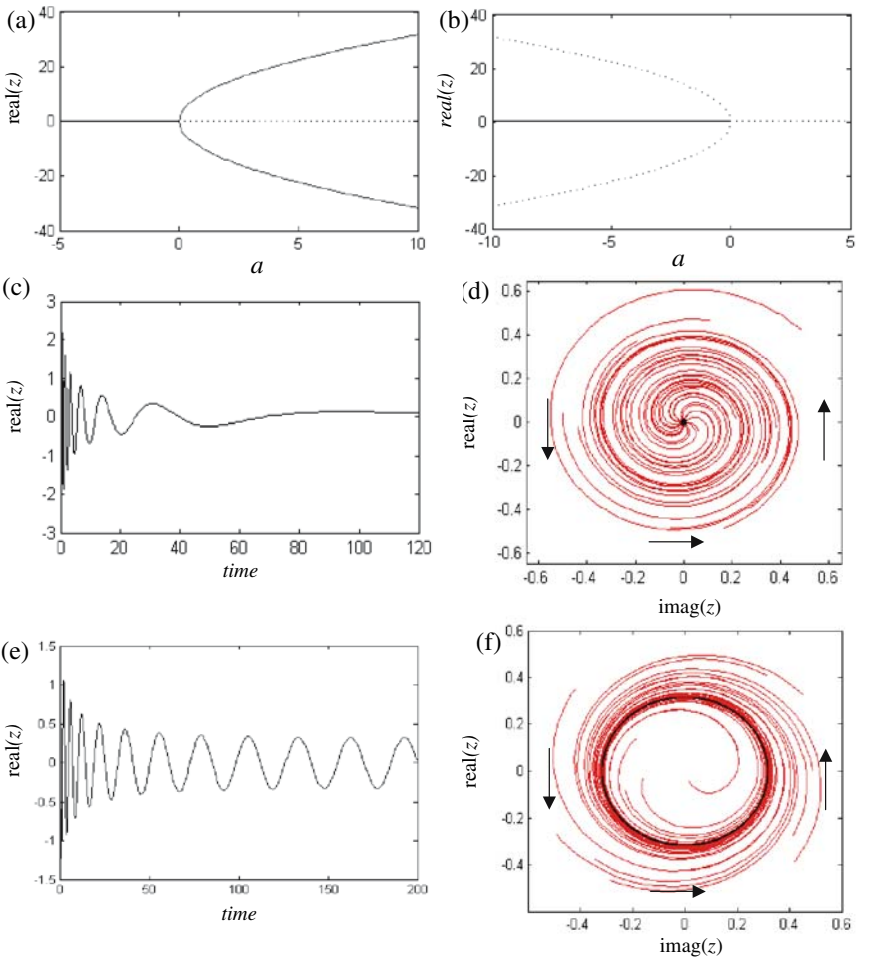

Fig. 11. Hopf bifurcation (**a**) Supercriticial, and (**b**) subcritical. Black line denotes fixed point attractor (solid) and repellor (dashed). Blue lines denote the maxima and minima of the limit cycle attractor (panel a; solid) and repellor (panel b; dashed). Time series (**c**) and phase space portrait (**d**) of the fixed point attractor (**e**) in the supercritical system (i.e. when $a < 0$ and $\text{real}(b) < 0$). Time series and phase space portrait (**f**) of the limit cycle attractor (**black**) in the supercritical system (i.e. when $a > 0$ and $\text{real}(b) < 0$). Red orbits show transients

Conversely, when the real part of b is positive then the system exhibits a ***subcritical Hopf bifurcation*** (Fig. 11b). For $a < 0$ there exists a single stable fixed point attractor (a spiral inset) and an unstable periodic orbit. Hence the phase space is partitioned: those initial conditions within the periodic orbit spiral in towards the fixed point; those initial conditions outside of the limit cycle diverge towards infinity. When $a > 0$, there exists an unstable

fixed point (a spiral outset). Hence all initial conditions (except $z = 0$) diverge towards infinity.

A subcritical Hopf bifurcation often occurs in the context of bistability, when there co-exists a large-amplitude limit cycle attractor. Above the bifurcation point $a > 0$, orbits diverge outwards from the fixed point repellor to this attractor. Below the bifurcation point $a < 0$, the limit cycle repellor (dashed blue curve in Fig. 11b) separates the basin boundaries of the fixed point attractor at the origin and the large-amplitude limit cycle attractor.

In summary, Hopf bifurcations are of very high importance for an understanding of neural activity as they explain the onset and nature of oscillatory behaviour. Supercritical Hopf bifurcations lead to the appearance of small amplitude periodic oscillations. Subcritical Hopf bifurcations result immediately in a large amplitude limit cycle.

Period-doubling bifurcations typically occur as a sequence of events subsequent to a Hopf bifurcation, following a further increase in the bifurcation parameter. The main panel in Fig. 7 shows period-doubling bifurcations in the logistic map between parameter values $a \sim 3.0$ and the onset of chaos at $a \sim 3.5$. The first period-doubling bifurcation (i.e. from a simple periodic oscillation to a period-2 oscillation) corresponds to the "excitation" of the limit cycle attractor into an invariant torus around which the attractor winds. Subsequent period-doubling bifurcations increase the number of times the attractor twists around the short axis of the torus every time it makes one complete revolution around the long axis.

A ***fold*** or ***saddle-node*** is an interesting and illustrative bifurcation. It occurs when a stable and unstable fixed point collide (see Fig. 12). Consider the equation,

$$\frac{dz}{dt} = a + z^2. \tag{29}$$

For $a < 0$ there are two fixed points, an attractor at $-\sqrt{-a}$ and a repellor at $+\sqrt{-a}$. As a approaches zero from below, these two fixed points hence approach each other and collide at $a = 0$. At this point, the fixed point, at $z = 0$, is attracting for $z < 0$ and repelling for $z > 0$. Hence it is neither an attractor nor a repellor, but rather a special ("non-hyperbolic") fixed point called a "saddle-node". The saddle node is classified as a local bifurcation because the two fixed points lose their asymptotic stability when they collide at $a = 0$. However, at $a > 0$ there is no fixed point – i.e. there is also a loss of structural stability. Hence it also meets the criteria for a global bifurcation.

A recently described phenomena is the ***blowout bifurcation*** (Ott & Sommerer 1994). Suppose we have two (n-dimensional) neural systems $z_1(t)$ and $z_2(t)$ evolving according to (11), each with chaotic dynamics. In the instance where there is no coupling ($c = 0$), the system as a whole explores the full phase space $\mathrm{R}^n \times \mathrm{R}^n$. When the system is strongly coupled ($c > c_k$ for some threshold coupling strength c_k), then the two systems will synchronize (Fujisaka & Yamada 1983, Pecora & Carroll 1990). In this case, the dynamics are confined to the 'hyper-diagonal' – that is, the space $z_1(t) = z_2(t)$ of half

the dimension of the full phase space. If the coupling strength c falls below c_k the dynamics of the two-cell system "blowout" from the low dimensional state of synchronization, into the full state space, as shown in Fig. 13. Alternatively, it can be said that when $c > c_k$ the state of synchronization has asymptotic stability. When c crosses c_k from above, the system loses stability in the direction transverse to the hyper-diagonal (Ashwin et al. 1996). Looking at the blowout bifurcation as c crosses c_k from below (i.e. as the coupling strength is increased) we see that – through the process of synchronization - the dynamics of the system collapse onto a (relatively) low dimensional manifold. That is, synchronization constrains the number of degrees of freedom of a spatially distributed dynamical system.

Global Bifurcations

Whereas local bifurcations deal with the loss of asymptotic stability of fixed points - and are hence concerned with the dynamics in local neighborhoods of attractors - global bifurcations can only be understood by studying the properties of the vector field outside of such neighborhoods. They occur when an attractor loses structural stability. Their nature depends upon the "skeleton" of the phase space – the nullclines, homoclines and heteroclines.

As stated above, a saddle-node bifurcation does have the properties of both a local and a global bifurcation in that there is no fixed point for $a > 0$. Looking at Fig. 12, we see that there are two fixed points when $a < 0$, an attractor at $-\sqrt{-a}$ and a repellor at $+\sqrt{-a}$. The latter forms the boundary of the basin for the former. Hence the bifurcation occurs when the attractor collides with its basin boundary. This collision illustrates the principles of more complex global bifurcations. An example, when a chaotic attractor collides with its fractal basin boundary was termed a ***crisis bifurcation*** when it was first described (Celso et al. 1982). More specifically, a ***boundary crisis*** occurs when the collision is between an attractor and a boundary, whereas an ***interior crisis*** results from the collision between an attractor and a saddle. The former results in the sudden loss of an attractor and its basin, whereas the latter typically leads to the sudden increase in the extent of the attractor.

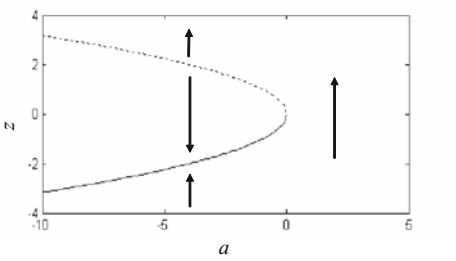

Fig. 12. Saddle-node bifurcation. Solid line denotes fixed point attractor. Dashed line denote fixed point repellors. Arrows show representative vector field

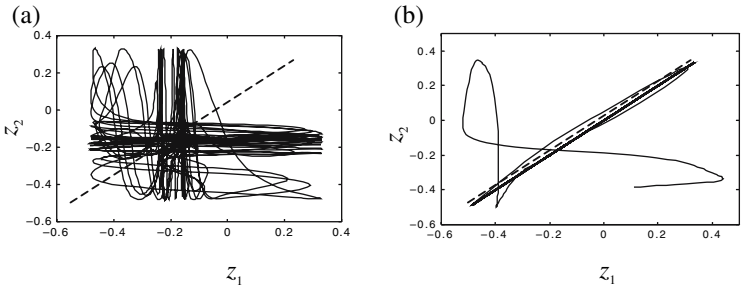

Fig. 13. Blowout bifurcation in system of two coupled logistic maps. (**a**) When $c < c_k$ the system explores R^2. (**b**) When $c > c_k$ the system contracts onto the diagonal after a brief transient. Arrow points to initial condition. A "blowout bifurcation corresponds to a transition from (**b**) to (**a**). Adapted from Breakspear (2004)

Other global bifurcations involve intersections of homoclinic or heteroclinic orbits either with themselves, or with fixed point attractors. A fascinating example involves the birth of a limit cycle out of a saddle-node bifurcation on a homocline! This obscure-sounding event actually lies at the heart of neuronal firing and we discuss it in more depth in the next section.

3 A Taxonomy of Neuronal Models

Neurons are traditionally seen as the building blocks of the brain. It hence makes sense to gain some insight into their dynamics – and functional interactions – at the microscopic scale at which they reside before moving into the larger scales, which we do in Sect. 4.

The "foundation stone" of microscopic models are the conductance-based Hodgkin-Huxley model and its derivatives. A full description of these is provided by a number of authors (e.g. Izhikevich 2005, Gerstner & Kistler 2002, Guevara 2003). Our objective here will be to quickly move from the full model to a two dimensional approximation and then explicate the onset of neuronal firing as a dynamical bifurcation.

3.1 The McCulloch-Pitts System

Before we do this, for the sake of theoretical and historical completeness, we briefly discuss the McCulloch-Pitts model (1943),

$$z(x_i, t+1) = S\left(\sum_j h_{ij} z(x_j, t) - \varepsilon_i\right), \tag{30}$$

where h_{ij} is the connectivity matrix, ε the "threshold" of neuron i and S is the step function. Neural inputs to a given unit are summed and then

converted into a binary output if they exceed the threshold ε_i. The resulting output is iteratively fed back into the network. Hence the McCulloch-Pitts model is discrete in both space and time, and as such is an example of a coupled difference map (5). Considered together with the use of the step function as representing neural "activation", this model is perhaps as abstract as possible. Nonetheless, McCulloch and Pitts proved that the system was capable of remarkably general computational feats. However, it is probably fair to say that this model finds its place more appropriately in the lineage of artificial neural networks than in the understanding of the dynamics of biological systems. Hence, McCulloch-Pitts systems form the basis for the two-layer "perceptrons" of Rosenblatt (1958) and the symmetric Hopfield (1982) networks. These extend the complexity and computational properties of McCulloch-Pitts systems to permit object categorization, content-addressable memory (i.e. the system correctly yields an entire memory from any subpart of sufficient size) and learning. For example, Sejnowski and Rosenberg (1987) showed that such systems, if constructed with three interconnected layers, are able to learn language pronunciation.

An overview of related advances is provided by Ermentrout (1998). For a fascinating history of this model and the life of Walter Pitts, see Smalheiser (2000).

3.2 Biophysical Models of the Neuron: The Hodgkin-Huxley Model

Whereas the McCulloch-Pitts system was constructed to embody only the very general network properties of neural systems and to directly address computational issues, the Hodgkin Huxley model aims to incorporate the principal neurobiological properties of a neuron in order to understand phenomena such as the action potential. Computational properties of these neurons are then investigated.

The paper of Hodgkin and Huxley (1952) is remarkable in that it casts detailed empirical investigations of the physiological properties of the squid axon into a dynamical systems framework. The Hodgkin-Huxley model is a set of conductance-based coupled ordinary differential equations[6] of the form of equation (8), incorporating sodium (Na), potassium (K) and chloride ion flows through their respective channels. Chloride channel conductances are static (not voltage dependent) and hence referred to as leaky (L). Hence we have,

$$C\frac{dV(t)}{dt} = g_{Na} f_{Na}(V(t)) \times (V(t) - V_{Na}) + g_K f_K(V(t)) \times (V(t) - V_K) + g_L \times (V(t) - V_L) + I, \tag{31}$$

where $c = 1\ \mu\mathrm{F/cm}^2$ is the membrane capacitance, I is an applied transmembrane current and V_{ion} are the respective Nernst potentials. The

[6] Here we depart slightly from the traditional nomenclature in order to simplify the mathematical description of the model.

coefficients g_{ion} are the maximum ion flows in the case where all the channels of that ion species are open. The Na and K ion flows reflect the state of "activation" channels, which open as membrane voltage increases and "inactivation" channels, which close. These are given by,

$$f_{Na}(V) = m(V)^M h(V)^H$$
$$f_K(V) = n(V)^N \tag{32}$$

where m and n are activation channels for Na and K, and h is the single inactivation channel for Na. The exponents are determined by the number of such classes of channel $M = 3$, $H = 1$ and $N = 4$. Hence (31) reflects the combined flow of all ion species as they are "pushed through" open channels according to the gradient between the membrane and Nernst potentials.

The kinetics of activation and inactivation channels are determined by differential equations of the form,

$$\frac{dm(V)}{dt} = \frac{(m_\infty(V) - m(V))}{\tau_m(V)} \tag{33}$$

where $m_\infty(V)$ is the fraction of channels open if the voltage is kept constant and $\tau_m(V)$ is a rate constant. These are determined empirically. These equations embody the exponential relaxation of channels towards their (voltage-dependent) steady states $m_\infty(V)$ consequent to a transient change in membrane potential. The kinetics of h and n are of the same form, although their rate constants τ are obviously distinct. The form of $m_\infty(V)$ – the steady state configurations of ion channel populations as a function of membrane potentials – is sigmoid shaped of the form,

$$m_\infty(V) = \frac{m_{\max}}{1 + e^{(V_m - V)/\sigma}}. \tag{34}$$

where V_m is the threshold potential for the ion channel and σ introduces the variance of this threshold. Figure 14 summarizes membrane dynamics in the Hodgkin-Huxley model.

The Hodgkin-Huxley model is a conductance approach to the dynamics of neural activity, reflecting ion flows through voltage- and time-dependent transmembrane channels. It represents a beautiful juncture of empirical and mathematical analysis. It not only offers an explanation of neural firing, but it quantitatively captures the complex shape of a neural depolarization.

3.3 Dimension Reductions of the Hodgkin-Huxley Model

The Hodgkin-Huxley model is able to explain the chief properties and many of the nuances of neuronal depolarization, including the threshold effect and the post-depolarization refractory period with quantitative accuracy. However, much of the qualitative (and some of the quantitative) behaviour can be

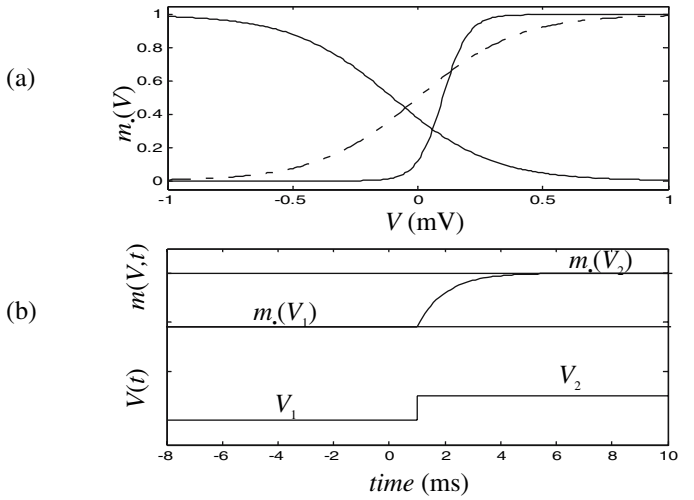

Fig. 14. Transmembrane currents in the Hodgkin-Huxley model. (**a**) Three examples of the sigmoid relationship between transmembrane potential V and steady state conductances $m_.$. Solid and dotdashed lines denote "activation" channels (such as m and n) whereas the dashed line denotes an inactivation channel (such as h) (**b**) Exponential "relaxation" of transmembrane conductance according to (33), following a discrete change in the transmembrane potential (lower line). Conductance m 'relaxes' from $m_.(V_1)$ to $m_.(V_2)$

captured by greatly reduced approximations. Amongst other things, first pass approximations ignore the voltage-dependent nature of τ_m and make further simplifications, but are still able to capture many of the important dynamics, such as neural depolarization. We now describe these, following the basic approach of Izhikevich (2005).

Morris-Lecar and Related 'Planar' Simplifications

An essential ingredient of a neural firing is a fast depolarizing current such as Na^+ – which is turned on subsequent to a synaptic current - and a slow repolarizing current such as K^+ - which restores the resting membrane potential. These in turn are facilitated by the existence of slow and fast ion channels of the respective species, $\tau_m(V) << \tau_n(V)$. The depolarizing current represents positive feedback (i.e. is self promoting) and, if a threshold is reached before a sufficient number of slower K^+ channels are open, the cell depolarizes. By contrast, the Na^+ inactivation channel plays less of a "brute force" role and can be ignored. The requirement of a "fast" depolarizing current and a slow repolarizing current can be met in a two dimensional ("planar") system,

$$\frac{dV}{dt} = g_{Na} m_\infty (V) \times (V - V_{Na}) + g_K n (V) \times (V - V_K) + g_L \times (V - V_L) + I, \tag{35}$$

where the dynamics of the slow repolarizing K^+ is given by

$$\frac{dn}{dt} = \frac{(n_\infty - n)}{\tau_n} \tag{36}$$

and the steady state currents given by,

$$n_\infty(V) = \frac{n_{\max}}{1 + e^{(V_n - V)/\sigma}}, \qquad \text{and} \qquad m_\infty(V) = \frac{m_{\max}}{1 + e^{(V_m - V)/\sigma}},$$

In other words, fast sodium channels *instantaneously* assume their steady state values following a change in membrane potential, hence adapting in a step-wise manner to a step-like change in membrane potential. Hence there is no differential equation for the Na^+ activation channels, m. This is exactly the form of the Morris-Lecar model, with the exception of a substitution of Na^+ currents with Ca^{++}.

The system (35)–(36) is known as planar, as its phase space is the two-dimensional plane spanned by V (the abscissa) and n (the ordinate). To understand the dynamics we calculate the nullclines for the dynamical variables V and n. The V-nullcline, obtained by substituting $\mathrm{d}V/\mathrm{d}t = 0$ into (35) is,

$$n = \frac{I - g_{Na} m_\infty(V) \times (V - V_{Na}) - g_L \times (V - V_L)}{g_K \times (V - V_K)}. \tag{37}$$

Similarly, the n-nullcline, obtained by setting $\mathrm{d}n/\mathrm{d}t = 0$ is,

$$n = \frac{n_{\max}}{1 + e^{(V_n - V)/\sigma}}, \tag{38}$$

These nullclines for the parameter values given in Table 1 and synaptic current $I = 0$ are plotted in Fig. 15. We see that there are three nullclines crossings corresponding to three fixed points, $\{-66, 0\}$, $\{-56, 0\}$ and $\{-25, 0.5\}$. Stability analysis shows that these fixed points are a stable focus, saddle point and spiral outset respectively (Izhikevich 2005). Hence the first fixed point first represents the only stable (steady state) solution.

Figure 15(b) shows two heteroclines – that is, outsets of the saddle point that become insets of the stable node. A long heteroclinic (magenta) traverses the nullclines before reaching the node whereas the shorter one (yellow) is able to track in parallel to the n-nullcline directly between the fixed points.

Table 1. Parameter values for the planar system (37)–(38) and figures 15–19

Capacitance,	$C = 1$;
Synaptic current (default),	$I = 0$;
Leaky channels:	$V_L = -80;\ g_L = 8;$
Sodium channels:	$V_{Na} = 60;\ g_{Na} = 20; V_m = -20; \sigma_m = 15; m_{max} = 1;$ $\tau_m = 1;$
Potassium channels:	
"high threshold"	$V_K = -90;\ g_K = 10;\ V_n = -25;\ \sigma_n = 5;\ n_{max} = 1;\ \tau_n = 1;$
"low threshold"	$V_K = -78;\ g_K = 10;\ V_n = -45;\ \sigma_n = 5;\ n_{max} = 1;\ \tau_n = 1;$

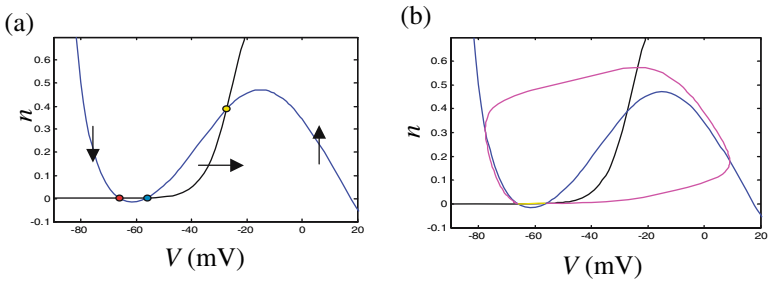

Fig. 15. Fixed points and nullclines of the planar system (37)–(38). The V-nullcline (39) is given in blue and the n-nullcline (eqn 40) in black. (**a**) Fixed points occur at the intersections of the nullclines: Stable node (red), saddle point (blue) and spiral outset (yellow). Arrows show representative vector field. (**b**) Long (magneta) and short (yellow) heteroclines of stable node and saddle

In Fig. 16 is shown representative orbits of this system. Three "subthreshold" (green) and three "suprathreshold" (red) orbits are shown. In the latter case, the neuron depolarizes before returning to its resting state. It should be noted that this threshold depends not only on the initial membrane potential V but also the initial K^+ membrane conductance. The separatrix between sub- and supra-threshold is constituted by the inset of the saddle point (not shown).

Whether the initial condition is sub- or supra-threshold, this system only has a single steady state solution in the current parameter regime. Hence, after at most one depolarization, it enters a quiescent state. Thereafter a discrete synaptic input, such as due to an excitatory post-synaptic potential (EPSP), will trigger a further discharge only if it is of sufficient strength to 'knock' the system over the inset of the saddle point. This will hence determine whether the resulting neural response is of the green or red waveform as in Fig. 16.

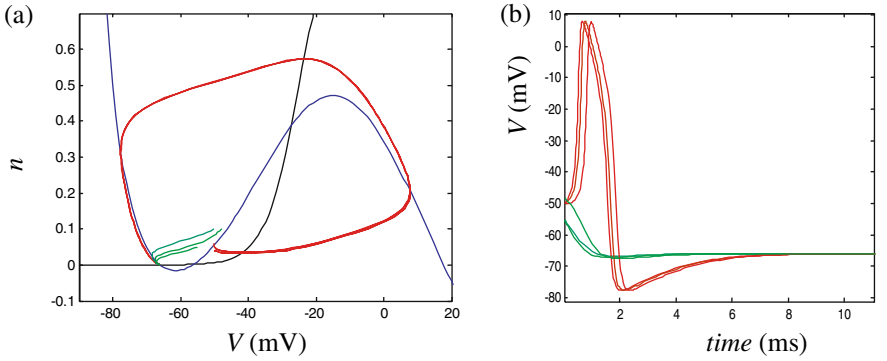

Fig. 16. (**a**) Representative sub- (green) and supra-threshold orbits (red) and (**b**) their temporal evolution

Bifurcations and Neuronal Firing in Planar Models

Saddle-node bifurcation

A further examination of the equation for the V-nullcline (37) shows that the synaptic current is a purely additive term. It hence acts to translate this nullcline in the vertical direction, with no influence on its shape and no influence on the n-nullcline. In Fig. 17, a close-up of the nullclines is shown for values of $I = 0$, 2, 4.51 and 6. As I is increased from 0 to 2 (dot-dashed), we see an upward shift of the V-nullcline so that the saddle and node fixed points are closer together in phase space. At $I = 4.5$ (dashed), the nullclines are tangent and the fixed points have hence collided. At $I = 6$ (dotted) there are no nullcline intersections: hence their collision has led to their mutual annihilation!

This is exactly the "saddle-node" bifurcation defined at Fig. 12. In the present setting, the synaptic input I functions as the bifurcation parameter. However, in addition to the structure of Fig. 12, an additional "global" feature of the phase space in the current system requires consideration. When the fixed points collide, the short heteroclinic is abolished, but the long heteroclinic[7] remains (Fig. 17b). Indeed even when $I > 4.51$ this orbit is still an invariant of the dynamics. However, with no fixed point along its domain, it is now a continuously looping limit cycle.

Figure 18 shows the limit cycle attractor (red) and its temporal dynamics for $I = 4.75$ (top row) and $I = 6$ (bottom row). Note that although the phase space portraits look similar, the frequency of the dynamics increases substantially with the increase in synaptic current.

This can be understood as a consequence of the bifurcation. Just after the bifurcation, although the nullclines do not intersect, the limit cycle must pass

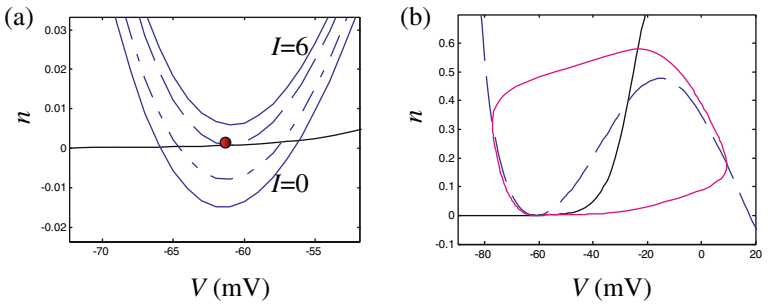

Fig. 17. Saddle-node bifurcation in the planar system. (**a**) Nullclines near fixed points for $I = 0$, 2, 4.51, 6. Red circle denotes "saddle-node" fixed point (**b**) Homoclinic orbit for the system when $I = 4.51$

[7] In fact, as there exists only a single fixed point, this orbit is more accurately now a "homocline".

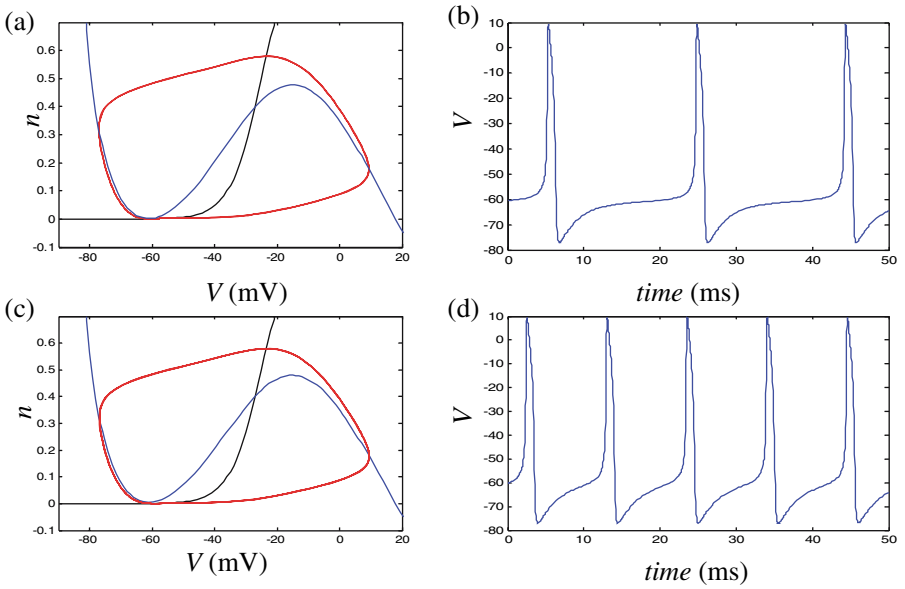

Fig. 18. Limit cycle dynamics for $I = 4.75$ (top row) and $I = 6$ (bottom row)

through a very narrow gap between them. The vector field in this gap bears the "memory" of the fixed points – namely it is very slow. Hence the orbits in this vicinity are near-stationary, as can be seen in the time domain. As I increases this influence diminishes and the frequency hence increases. Note that in both cases, however, there is virtually no change in the morphology of the depolarization, which is not related to this phenomenon.

Hopf bifurcation

Through a slight change in the parameters relating to the potassium channels, however, the transition from steady state (fixed point) to periodic (limit cycle) dynamics can occur through a different type of bifurcation. In the above scenario the potassium channels had values consistent with a "high threshold", namely the mean threshold potential of the K^+ potassium channels $V_n = -25\,\text{mV}$. Lowering V_n to $-45\,\text{mV}$ and changing the Nernst potential to $V_K = -78\,\text{mV}$ yields the phase space portraits and time series plotted in Fig. 19.

Firstly, there is only one interception of the nullclines for these parameter values, and hence only one fixed point. For $I < 19$ this is a spiral inset, hence yielding damped oscillations (panels a,b). For $I > 19$ the fixed point has undergone a (supercritical) Hopf bifurcation, hence yielding a small amplitude limit cycle, coinciding with sustained but subthreshold voltage oscillations. For $I \sim 26$, the amplitude of these oscillations grows smoothly but rapidly so that with $I = 27$ the system exhibits sustained suprathreshold oscillations. However, note that the damped, subthreshold and suprathreshold oscillations

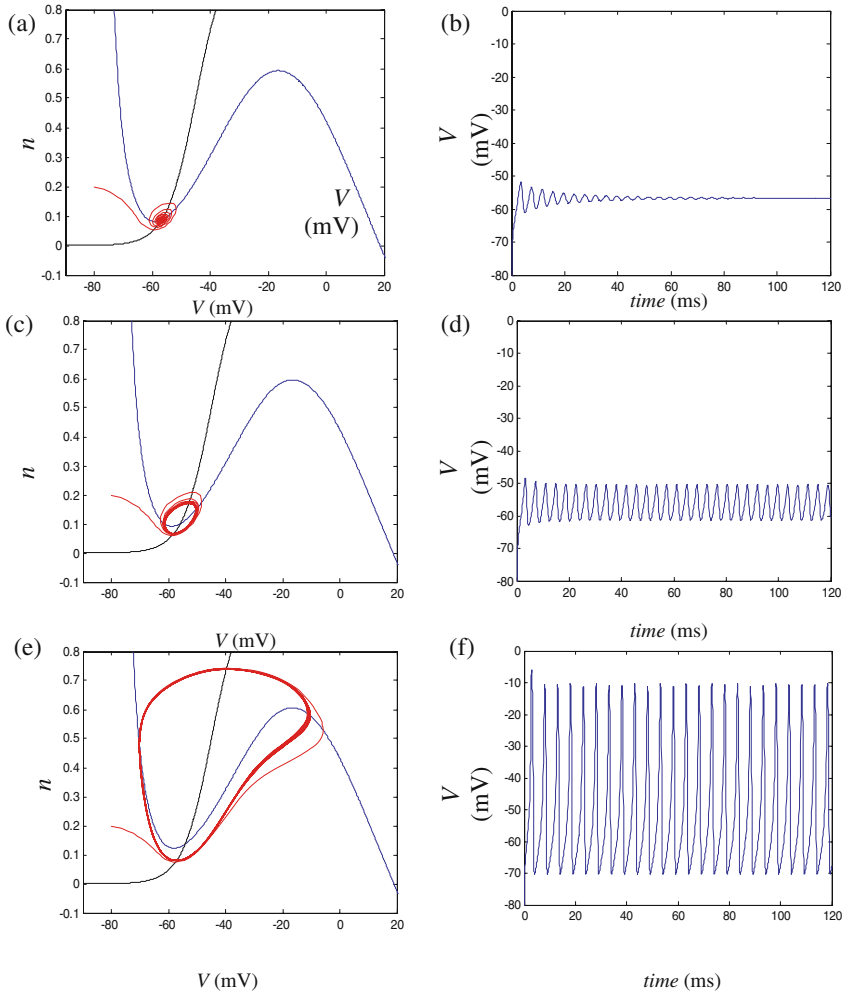

Fig. 19. Phase portrait and time series of the planar model in the "low K^+ threshold" case for $I = 18.5$ (top row), $I = 21$ (middle row) and $I = 27$ (bottom row)

all have approximately the same frequency. This contrasts with the saddle-node scenario.

We conclude with the two different bifurcation sets, Fig. 20, corresponding to distinct routes to sustained oscillations in this neuronal model. Panel (a) shows the saddle-node bifurcation, yielding the sudden onset of suprathreshold oscillations at $I \sim 4.5$ mA. Panel (b) depicts the Hopf bifurcation with the gradual onset of subthreshold oscillations at $I \sim 19$ mA, growing rapidly to suprathreshold with $I \sim 26$ mA.

In the presence of discrete synaptic inputs, the saddle-node system will generate an all-or-nothing depolarization – or chain of depolarizations – if

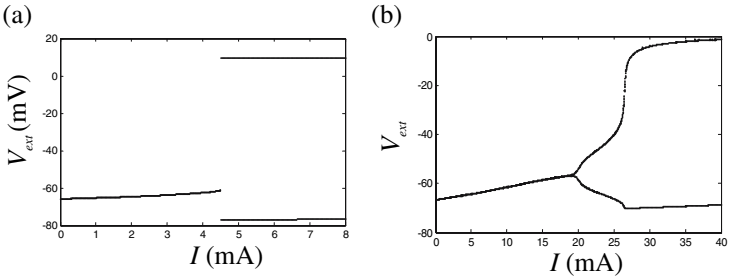

Fig. 20. Saddle-node (**a**) and (**b**) Hopf bifurcation diagrams for the planar neural system with high and low K^+ channel thresholds, respectively

the input is sufficiently large. The frequency of any such chain of discharges increases with the magnitude of the synaptic input. On the other hand, the Hopf route will generate either damped, sub-threshold oscillations or a chain of depolarizations, although the frequency of these will be more-or-less constant. In the presence of discrete synaptic inputs, the saddle-node system will generate an all-or-nothing depolarization – or chain of depolarizations – if the input is sufficiently large. The frequency of any such chain of discharges increases with the magnitude of the synaptic input. On the other hand, the Hopf route will generate either damped, sub-threshold oscillations or a chain of depolarizations, although the frequency of these will be more-or-less constant. As discussed in Izhikevich (2005) these two distinct neuronal responses to applied (or synaptic) currents were first observed empirically by Hodgkin in the 1940's. Specifically, he classified neurons that showed a frequency-dependence on the size of the synaptic current (i.e. Hopf-like responses) as *Type I neurons*. In particular, for small currents, these neurons begin to fire at very slow frequencies. In contrast, those neurons that start firing at relatively rapid rates following a supra-threshold input – and which show very little further increases in frequency – were classified as *Type II neurons*. The squid axon described by the original Hodgkin-Huxley model (1952) is a representative example of a neuron with type II behavior.

The FitzHugh-Nagumo Model

As we have seen above, the shape and intersections of the nullclines plays the determining role in the behavior and bifurcations of the dynamics. In fact, all that is required to reproduce the qualitative nature of the dynamics is the cubic-like shape of the V-nullcline and the presence of an n-nullcline with the appropriate intersections. Mathematically, these requirements can be met with the much simpler algebraic equations (FitzHugh 1961, Nagumo et al. 1962),

$$\frac{dx}{dt} = x\,(a - x)\,(x - 1) - y + I, \qquad \frac{dy}{dt} = bx - cy, \tag{39}$$

which have the simple nullclines,

$$y = x\,(a - x)\,(x - 1) + I, \qquad y = {}^{b}\!/_{c}\,x, \tag{40}$$

In Fig. 21 is illustrated a phase portrait and time series for this system following a super-critical Hopf bifurcation of the single fixed point. This system - and variations of it - are known as the FitzHugh-Nagumo model.

This system hence allows a closed-form analysis, with relatively simple algebraic forms, of the same qualitative phenomena as the planar model of Hodgkin-Huxley dynamics.

The Hindmarsh-Rose Model

The Hindmarsh-Rose model is the last in the "microscopic" domain for consideration. It continues the logic of the FitzHugh Nagumo model – namely that it captures the qualitative essence of neuronal firing through a simple algebraic form of the evolution equations (and hence of the nullclines). However, rather than further reducing the Hodgkin-Huxley model, the Hindmarsh-Rose (1984) model introduces an extra property. The system is given by,

$$\frac{dx}{dt} = y - ax^3 + by^2 - z + I, \tag{41}$$

$$\frac{dy}{dt} = c - dx^2 - y, \tag{42}$$

$$\frac{dz}{dt} = r\,[s\,(x - x_0) - z]\,, \tag{43}$$

When $r = 0$, the third variable plays no role and the system reduces to a variation of a FitzHugh Nagumo model – that is, a two dimensional spiking neuron with a simple algebraic form: An example is given in Fig. 22.

However, setting $r > 0$ but small has the effect of introducing the third variable into the dynamics. Notice that z only enters into the first two

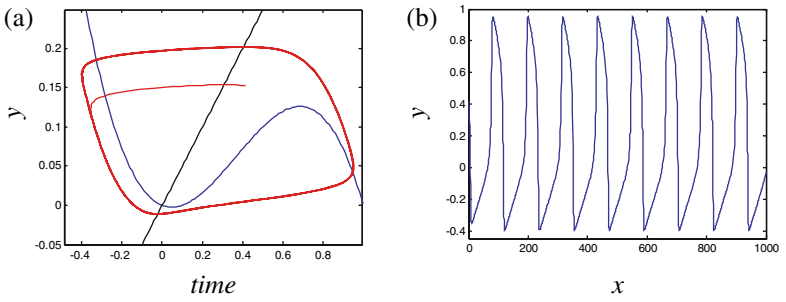

Fig. 21. Phase portrait and time series for the Fitz-Hugh-Nagumo model following a Hopf bifurcation. Parameters, b = 0.01; c = 0.02; a = −0.1; I = 0.1 as per Izhikevich (2005). Note the qualitative similarity to Fig. 19(e), (f)

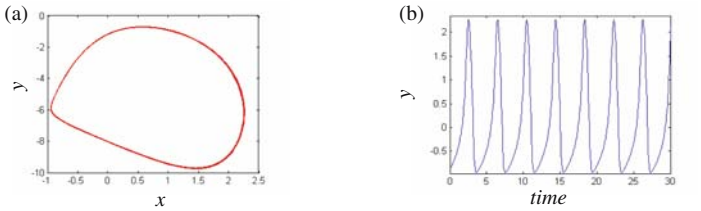

Fig. 22. Phase portrait and time series for the Hindmarsh-Rose model. Parameters, I = 3.2; a = 1.0; b = 3.0; c = 1.0; d = 5.0; s = 4.0; x0 = −1.60; r = 0

equations as an additive term – the same as I although negative in size. Also, setting r small has the effect of ensuring that z evolves on an intrinsically slower time scale than x and y. Together, these constructions have the effect of ensuring that z acts like a slowly varying synaptic current, albeit one which, due to the x term in (45), is also state dependent. Hence as z becomes more negative, it acts like the bifurcation parameter in the FitzHugh Nagumo model and precipitates – via a subcritical Hopf bifurcation - a run of depolarizations. However, due to the x term in (43), these depolarisations have the (relatively slow) effect of increasing z. Eventually the depolarizations are terminated as the reduced effective contribution of z to total synaptic current restabilizes the fixed point via a saddle node bifurcation. Hence the system, as shown in Fig. 23, exhibits a burst of spikes interspersed by quiescent phases. Indeed with $r = 0.006$, the system exhibits this pattern in a chaotic fashion.

Note that, as discussed, the fast spikes are far more evident in the dynamics of x whereas the dynamics of z are more sensitive to the bursts.

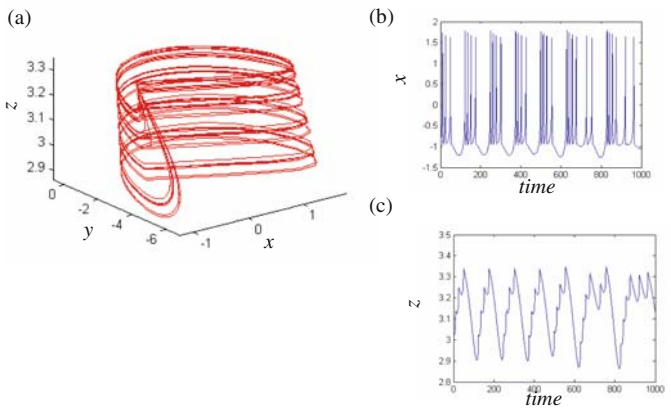

Fig. 23. Phase portrait (a) and time series (b,c) for the Hindmarsh-Rose model. Parameters, I = 3.2; a = 1.0; b = 3.0; c = 1.0; d = 5.0; s = 4.0; x0 = −1.60; r=0.006

Such burst-spiking is of particular interest to classes of thalamic neurons and many cortical neurons during slow-wave sleep, whereby this activity is observed synchronously across the scalp (McCormick & Bal 1997). Interactions between such systems can be introduced by coupling of one of the fast variables, such as

$$\frac{dx_{1,2}}{dt} = y_{1,2} - ax_{1,2}^3 + by_{1,2}^2 - z_{1,2} + I + C\left(x_{2,1} - x_{1,2}\right), \tag{44}$$

where C is the coupling parameter. Two such simulations are shown in Fig. 24, where blue and green time series denote each system. In the top row, with $c = 0.35$, the bursts are coincident but the spikes are often discordant. However with $c = 0.5$, the spikes are also synchronized. This interesting phenomenon, studied in detail by Dhamala et al. (2004) of burst and then spike synchrony, has been observed experimentally.

3.4 Coupled Chaos in a Mesoscopic Model

The Hindmarsh-Rose model introduces an extra term, incorporating a slow calcium current, into a planar model of an excitable neuron. An alternative extension of planar models is to introduce a single variable representing a feedback from an inhibitory neuron Z. The inhibitory and excitatory neurons interact via synaptic currents induced through their mutual connectivity. Such a model takes the form (e.g. Larter et al. 1999),

$$\begin{aligned}\frac{dV}{dt} &= g_{Na}m_\infty(V) \times (V - V_{Na}) + g_K n(V) \times (V - V_K) + g_L \times (V - V_L) \\ &\quad + \alpha_{ne}I + \alpha_{ie}F(Z), \\ \frac{dn}{dt} &= \frac{(n_\infty - n)}{\tau_n}, \qquad \frac{dZ}{dt} = \alpha_{ei}G(V) + \alpha_{ni}I. \end{aligned} \tag{45}$$

Local connectivity is parameterized by the coupling parameters α between inhibitory Z, and excitatory V cells and via input from the external noise

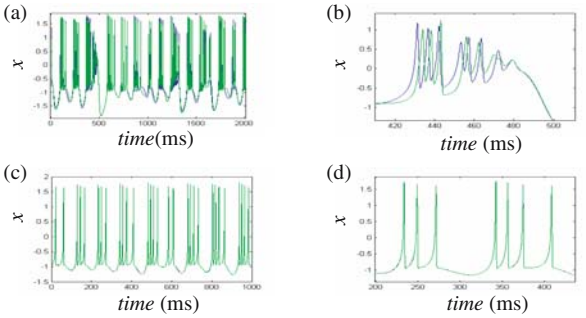

Fig. 24. Coupled Hindmarsh-Rose systems with $c = 0.35$ (top row) and $c = 0.5$ (bottom row)

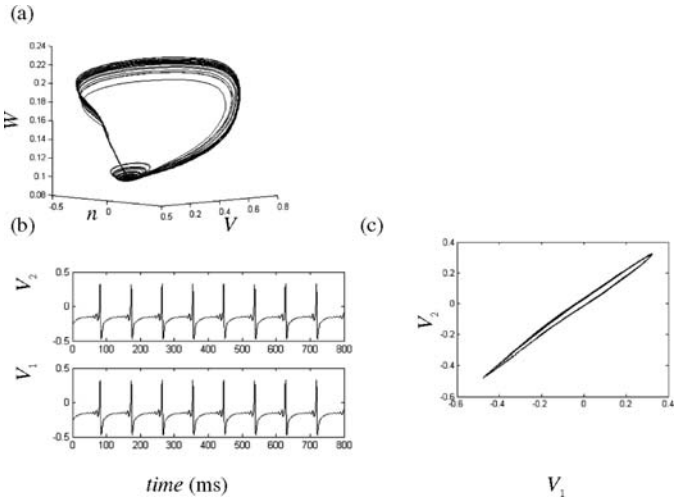

Fig. 25. Generalized chaotic synchronization in a mesoscopic neuronal model. (**a**) Chaotic attractor. The orbits are organized around a manifold that is homoclinic to the unstable spiral (**b**) Time series of excitatory membrane potentials in two coupled systems showing apparent synchronization. (**c**) Their co-evolution shows a smooth manifold slightly off the state of identical synchrony $V_1 = V_2$

term I. The functions F and G model the feedback between the inhibitory and excitatory cells. Within physiologically realistic parameter values, such a system can exhibits chaotic dynamics, as shown in Fig 25 (a), organized around a homoclinic orbit.

Synaptic coupling between the excitatory neurons in two such populations of cells allows construction of a ***mesoscopic*** neuronal model – a system on the intermediate scales between single neurons and the large scale systems considered in the following section. An example of synchronization between two such subsystems is illustrated in Fig. 25 (b-c), where a single parameter in each system has been set with a small mismatch (all other parameters are equal). Whilst the time series appear identical (panel b), a plot of the values of V_1 versus V_2 (panel c) reveals that their co-evolution, whilst close to the diagonal is nonetheless confined to a nearby smooth manifold. This form of non-identical synchronization is known as ***g***eneralized chaotic synchronization (Afraimovich et al. 1986, Rulkov et al. 1995). Further details and examples of more complex behaviors – such as intermittency, scale-free dynamics and travelling waves - can be found in Breakspear et al. (2003, 2005).

This concludes our survey of basic, small-scale neural systems. We hope to have illustrated the power of combining analysis and geometry in elucidating some of the fundamental properties of neurons. We now turn to macroscopic models.

4 From Small to Large Scale Models

Large scale neural network models are thought to be involved in the implementation of cognitive function of the brain (Mesulam 1990; Bressler 1995, 2002, 2003; Bullmore et al. 1996; Mountcastle 1998; McIntosh 2000; Bressler & Kelso 2001; Jirsa 2004; Bressler & Tognoli 2006; Bressler & McIntosh 2007). To understand the neural basis of cognition, theoretical and analytical means must be developed which are specifically targeted to the properties of large scale network dynamics. Such theoretical understanding will also guide the interpretation of the enormous data sets obtained from non-invasive brain imaging. The functional expression of a cognitive operation seems to require the co-activation of certain subnetworks. Such co-activation does not necessarily require a simultaneous activation of all network components, but may be represented in a characteristic spatio-temporal network dynamics with both simultaneous and sequential activations. The properties of the network dynamics will crucially depend on the interconnectivity of the network components and their dynamics (Sporns 2002; Sporns & Tononi 2002, 2007; Jirsa 2004; Beggs et al. 2007). The goal of any large-scale description of neural dynamics is to reconstruct all relevant spatiotemporal dynamics of the neural system while preserving the mechanisms which give rise to the observed dynamics. Large scale models have the implicit assumption to be based upon neurocomputational units, which are more macroscopic than single neurons. This approach is to be juxtaposed with the high-dimensional computation of the full network composed of microscopic complex neurons with dendritic and axonal ion channel dynamics, as well as pre- and postsynaptic processes. Large scale models also bear the promise that they provide insight into the underlying dynamics-generating mechanisms of the network due to their reduced complexity. Finally, large scale models are easier and less time-consuming to be solved computationally. The following sections discuss the various schools of thought in large scale network modeling and characterize these from the perspective of anatomical and functional connectivity, the latter identified with the dynamics of the network.

4.1 Non-reducible Dynamics of Neuronal Ensembles

A large scale model is composed of microscopic units or atoms which do not represent individual neurons, but rather complexes, also referred to as ***neural masses*** (Beurle 1956), capturing the non-reducible dynamics of a set of neurons. Such complexes may either be localized in physical space and defined in a volume element at a location x, or distributed over physical space and are defined functionally (e.g. in K-sets as discussed below (Freeman 1975, 1992)). Though the former is more common, in practice the two variants often coincide due to stronger local connectivity and the resulting co-activations ("what wires together, fires together"). Unlike many subcortical structures, in which neurons are packed into nuclei, the cortical

sheet appears at first sight as a dense homogeneous medium with no obvious demarcation of its components. Corticocortical columns typically consist of 5,000 to 10,000 neurons, macrocolumns contain 10^5 to 10^6 neurons (Nunez 1995). Yet, there are a number of anatomical tracing studies which indicate mutual anatomical and functional parcellation (Szentagothai 1975; Mountcastle 1978). For instance, macrocolumns form functional units in sensory areas with homogeneous tuning properties inside the unit, but sharp differences amongst neighboring units (Mountcastle 1978). For our purposes, the neural mass is a highly connected set of neurons, sharing common input and output pathways and specialized low-level function. The activity of a neural mass (also known as ***neural mass action***) in a large scale model is described by an m-dimensional vector variable $\Psi(x,t) = (\Psi_1(x,t), \Psi_2(x,t), \cdots, \Psi_m(x,t))$ at a discrete location x in physical space and a point t in time. The variable Ψ(x,t) is also referred to as a ***neural population, neural assembly*** or ***neural ensemble activity***. If the distance between neighboring neural masses is infinitesimally small, then the physical space x is continuous and Ψ(x,t) is referred to as a ***neural field***. Since the neural mass action is physically generated by the N neurons within the neural mass, there will be a mapping $\Phi : Z(x,t) \rightarrow \Psi(x,t)$, which unambiguously relates the high-dimensional neuron activity $Z(x,t) = (Z_1(x,t), Z_2(x,t), \cdots, Z_N(x,t))$ to the neural mass action Ψ(x,t). $Z_i(t)$ is the n-dimensional state vector of the i-th neuron with i= 1,...,N. For concreteness, a neural mass may contain N=10,000 neurons with n=2 in case of a FitzHugh-Nagumo neuron model. The situation is shown in the cartoon on the bottom of Fig. 26. Here a cortical sheet is shown which is decomposed into color-coded patches representing neural masses. Within a neural mass the local connectivity of a single neuron is illustrated through the density of its connections (red squares) which decreases with increasing distance. The partial overlap of the neural masses indicates that synaptic connections of a neuron may belong to different neural masses. The critical step in the development of a large scale model occurs through the mapping $\Phi : Z(x,t) \rightarrow \Psi(x,t)$ when the activity $Z(x,t) = (Z_1(x,t), Z_2(x,t), \cdots, Z_N(x,t))$ of a given neural mass is replaced by its neural mass action $\Psi(x,t) = (\Psi_1(x,t), \Psi_2(x,t), \cdots, \Psi_m(x,t))$ where $m << N$. The nature of this relation between neuron activity $Z(x,t)$ and neural mass action Ψ(x,t) will be generally non-trivial and involves a mean-field reduction which will be discussed in the next section. On the top of Fig. 26 the neural network dynamics is now captured by locally coupled neural mass actions Ψ(x,t) assigned to each neural mass at location $x = X_i$. Each neural mass is locally (as indicated at location X_5) and globally (as indicated at location X_1) connected.

Rather than solving the complete network for the state vectors $Z(x,t)$ of all neurons, now the large scale network can be solved using the neural mass action Ψ(x,t) as indicated in the following: A large scale model representation is successful if the large scale model simulation provides the same neural mass

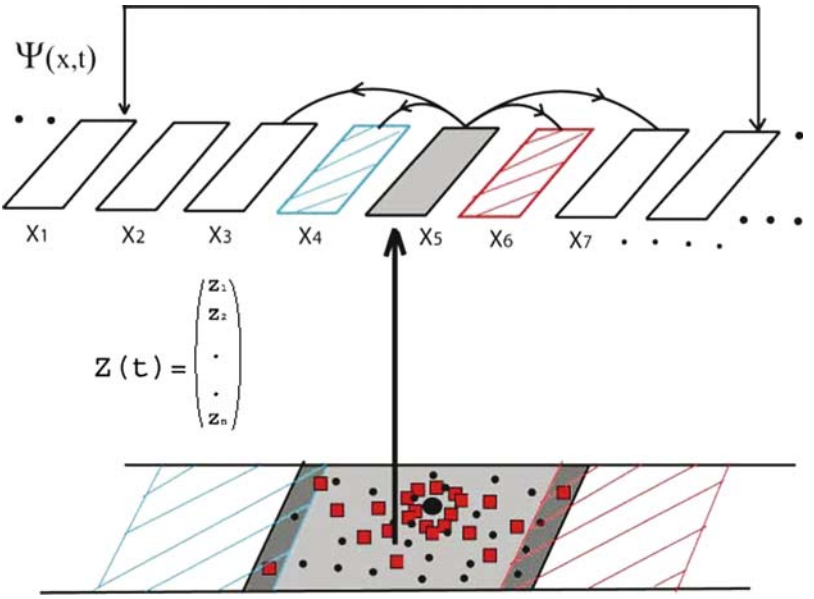

Fig. 26. Coupled neural masses at locations X_i (upper figure) are coupled via local and global pathways. The large scale network dynamics arises from the interactions of the neural mass actions $\psi(X_i, t)$ at locations X_i. The computation of the complete network dynamics based upon the neural state vector Z(t) (lower figure) and neural connectivity (red squares) should ideally yield the same network dynamics as computed from ψ(x,t)

action Ψ(x,t+T) at a future time point t+T as the simulation based upon the complete network dynamics using the microscopic neuronal activity Z(x,t).

$$\Phi : Z(x,t) \rightarrow \Psi(x,t) \xrightarrow{\text{large scale network dynamics}} \Psi(x,t+T) \leftarrow Z(x,t+T)$$

complete network dynamics

In the latter approach, once Z(x,t+T) is computed, it has to be mapped upon to the neural mass action, $\Phi : Z(x,t+T) \rightarrow \Psi(x,t+T)$ to allow for a comparison between the two approaches. The inverse mapping $\Phi^{-1} : \Psi(x,t+T) \rightarrow Z(x,t+T)$ generally does not exist.

4.2 Mean Field Reduction of Neuronal Activity

The ***mean field*** approximation is well-known from statistical physics (see for instance Gardiner 2004). Though its basic assumptions are mostly not rigorously justified, it often provides an astonishingly good qualitative insight into the description of many models. Hence the use of mean field approaches has

a long history in the field of neural networks. The mean field $u(t)$ is generally defined as the statistical expectation value E of a particular state variable. Two mean field approaches exist based on two opposing views of neuronal coding, but of course with many interim shades. The first view holds that the firing rate of a neural mass is relevant for neural information processing. The dissenting view posits that the information is encoded in the interactions among spikes and hence spike correlations must not be ignored (for detailed discussions of neuronal encoding see Koch 1999). In large scale models, neural mass action is mostly expressed by mean fields of firing rate, though also considerable evidence exists that single cells may fire spikes at predictable intervals as long as 200msec with a precision of 1msec (Abeles et al. 1993). The latter is the key observation leading to the theory of synfire chains for cortical processing (Abeles 1991). As of today, it is not clear to what degree the neural system uses firing rate or spike coding mechanisms. Experimental evidence exists for both and accumulates with every day (Koch 1999). In the following we elaborate on the import of both neural coding mechanisms to the field of large scale modeling.

Generally speaking, if the coupling is high enough and the parameter dispersion is sufficiently small, the neurons in the neural mass evolve in time close to each other within phase space (and hence to the mean field), or in other words are synchronized. Note however, that there are exceptions in the network dynamics literature known as oscillator death (see also Campbell 2007), in which the neural mass action becomes zero due to too strong coupling. A synchronized neural dynamics will play a lesser role for extended periods of time during which a large scale synchronization is more likely to indicate pathological network activity such as epilepsy (see Milton et al 2007, Ferree and Nunez 2007). However, the understanding of the conditions leading to the emergence of synchronization will likely be important to understanding the neurocognitive processes such as feature binding (Gray and Singer 1989; Crick and Koch 1990) and multisensory integration (Von Stein et al 1999; Treisman 1996). In fact, the onset of coherent oscillatory activity has been interpreted to be fundamental for the formation of higher-order percepts (Freeman and Skarda 1985; Bressler 1990). In the opposite case for small coupling and greater noise strength, the elements of the population move incoherently and eventually their positions average out. Here the asymptotic dynamics of the mean field is mostly characterized by the fluctuations and the mean firing rate. Between these two limit cases, complex behavior arises and can be addressed starting from either end of the limit.

Fluctuation dominated network dynamics and firing rate models

For small enough and sparse couplings, as well as sufficient noise within the neural mass, the neuronal action potential generations and the connectivity within the neural mass can be assumed to be independent. Under these conditions, all spike correlations will be destroyed and a ***firing rate model***

becomes a valid representation of neural mass action (Abbott & van Vreeswijk 1993; see Cessac & Samuelides 2006 for a review). In the limit of large neuron numbers within the mass, N→∞, and low firing rates, the total spike train, obtained by summing over the spike trains from all neurons within the mass, will be a Poisson point process with a common instantaneous firing rate ρ(x,t). Equivalently, the synaptic input I_s to a single neuron can be approximated by an average firing rate ρ(x,t) plus a fluctuating Gaussian contribution. As a consequence the joint probability distribution factorizes and a complete description of the neural mass action is obtained in terms of the first and second order statistical moments. Two further more subtle distinctions can be made. Either the firing rate ρ(x,t) plus Gaussian noise is used as synaptic input and the neural mass action is described by the average value of neural activity (the mean field) $u(t) = E[Z_i(t)]$ and the variance $v(t) = E\left[Z_i(t)^2\right] - u^2(t)$. Such finally results in Fokker-Planck approaches which describe the time evolution of the probability *P(Z(x,t),t)* to find a neuron at x and t in the state Z (Amit & Brunel 1997; Brunel 2000; Brunel & Hakim 1999; Cai et al. 2006). Alternatively, the neural mass action can be expressed directly by the mean firing rate $u(t) = E[\rho(t)]$ and its variance $v(t) = E\left[\rho(t)^2\right] - u^2(t)$ (Abbott & van Vreeswijk 1993; Nykamp & Tranchina 2000, 2001; Eggert & van Hemmen 2001). Note that we dropped the explicit dependence on x to simplify our notation. The mean field variables u and v define the 2-dimensional population vector $\Psi(x,t) = (u(t), v(t))$ at the location x. As long as the independence condition within the neural mass holds, the reduced dynamic description through Ψ(x,t)=(u(t),v(t)) is exact. The mean firing rate shows a sigmoid behavior as a function of the synaptic input, which can be intuitively understood as follows: a neural mass shall consist of independent neurons of which each displays a sharp onset of firing at a threshold value Θ (see Fig. 27).

The thresholds are independent and hence have a Gaussian distribution. The mean firing rate of the neural mass then becomes the well-known sigmoid function and has been carefully parameterized from experimental data of the olfactory bulb (Freeman 1975). Is the independence condition violated though

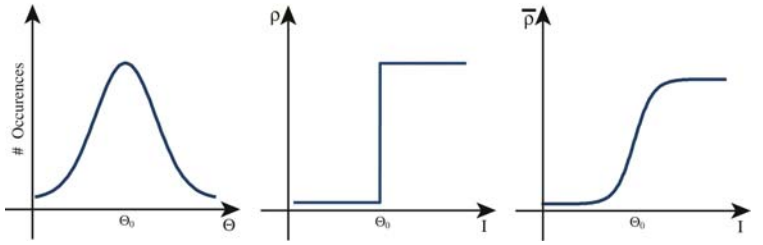

Fig. 27. Left: Gaussian distribution of activation thresholds within a neural mass. Middle: Sharp activation function (firing rate) of a single neuron acting as a threshold element. Right: Mean firing rate obtained from averaging all firing rates within a neural mass

and correlations are introduced, for instance through correlations within the connectivity weights via learning, the mean field approximation breaks down. Related in spirit to Fokker-Planck approaches, Ventriglia proposed a phenomenological kinetic theory for the study of the statistical properties of neural mass action (Ventriglia 1974, 1978). The kinetic equations capture the time course of the distribution function of the total excitation of a neural mass. The neurons in the mass are characterized by a level of inner excitation which changes when impulses are emitted. The impulses move freely within the neural mass and may be absorbed by other neurons changing their inner excitation level (see also by Gröbler et al. 1998; Barna et al. 1988 for extensions of the kinetic approach).

Synchronized network dynamics in population models

For strong coupling strengths and low level of noise within the neural mass, a different but complementary approach holds using the perfectly correlated state Z(t), that is $Z_1(t) = Z_2(t) = \cdots = Z(t)$. Or in other words, a special case of spike timing is considered: all neurons are synchronized and show the same dynamics $Z(t)$. DeMonte, d'Ovidio & Mosekilde (2003) proposed a method by which the mean field dynamics of a neural mass can be described by a low-dimensional population vector under conditions of global coupling and coherent neural mass action. Global coupling means that each neuron in the neural mass feels the same mean field activity. Their method applies to neural masses of any size and any type of intrinsic dynamics, as well as parameter dispersion. For example, if the underlying neuron model for $Z_i(t)$ is a FitzHugh-Nagumo Model, then the population vector $\Psi(x,t) = (\Psi_1(x,t), \Psi_2(x,t), \Psi_3(x,t), \Psi_4(x,t))$ is 4-dimensional where $\Psi_1(x,t), \Psi_2(x,t)$ describes the activity of an average FitzHugh-Nagumo neuron and $\Psi_3(x,t), \Psi_4(x,t)$ measures the dispersion of both parameter and phase space. If the neurons desynchronize too much, then the approach of DeMonte et al. (2003) will fail by definition. If, after loss of synchrony, multiple clusters of coherent activity emerge in phase space instead, then it is possible to describe the neural mass action through multiple mean fields. Each of these mean fields captures a single cluster dynamics (Assisi, Jira & Kelso 2005). In cases of parameter dispersion, such emergence of cluster dynamics is common and well-suited for the approach by Assisi et al. (2005). If the constraint of global connectivity within the neural mass is dropped, richer dynamic phenomena become possible such as the appearance of spiral waves (Chu et al. 1994; see Milton 1996) and will be discussed in the next sections. Freeman (1975,1987) proposed another classification of neural mass action which allows spike correlations to be considered. He originally classified the activity of the neural masses into classes named K0, KI and KII sets (K for Katchalsky) according to their functional architecture. K-sets are composed of elements which affect the nature of dynamics including physical components such as the interconnected neurons, the neurochemical environment, etc., but also purely

functional components such as the connection topology, the input structure, etc. K0 sets represent the simplest functional architecture which can be viewed as the ensemble average of the activity of independent but similar neurons. In their simplest forms, KI sets are equivalent to two coupled K0 sets, KII sets are composed of K0 and KI sets. However, they are more generally defined and are in principle not always reducible to lower order K sets. In this notation, a K0 set corresponds to the 1-dimensional and hence scalar activity of a neural mass, Ψ(x,t), whereas KI and KII sets correspond to higher-dimensional vectors Ψ(x,t).

4.3 Composition of Neural Masses to Large Scale Models

Neural mass models sacrifice realism for a more parsimonious description of the key mechanisms of large scale dynamics. The benefit lies in the possibility of emulating non-invasively obtained brain imaging data such as EEG and MEG. Neural mass models (Beurle 1956; Lopes da Silva et al. 1974; Freeman 1975; Nunez 1974, 1995; van Rotterdam et al. 1982; Jirsa & Haken 1996, 1997; Jirsa et al. 1998, 2002; Robinson et al. 1997, 2002, 2001; Tagamets & Horwitz 1998; Steyn-Ross et al. 1999; Valdes et al. 1999; David & Frison 2003; Breakspear et al. 2006) are based upon this approach. Much of the complexity of the signals arises from the coordination of the interconnected neural masses rather than the intrinsic dynamics of the microscopic unit, the neural mass, of the large scale network. A neural mass at location x is locally connected to its neighboring neural masses and globally connected to far distant neural masses at locations x'. In the following, physical space is always assumed to be one-dimensional, $x \in \Re$, but the mathematical treatment formally extends trivially to two and three dimensions. Note that though the formal extension to higher dimensions is not difficult, new dynamic network phenomena such as spirals may emerge due to the higher dimension (see Nunez (1995) for a discussion of spherical geometries). If the network dynamics described by (17) were linear, then the mapping $\Phi : Z(x,t) \rightarrow \Psi(x,t)$ would result in the following large scale dynamics for the neural mass action Ψ(x,t) with $Q = N$ and $S = H$

$$\frac{d\Psi\left(x,t\right)}{dt} = Q(\Psi\left(x,t\right)) + \int\limits_{\Omega}\int\limits_{-\infty}^{t} h\left(x-x'\right) S\left(\Psi\left(x-x',t-t'\right)\right) dt'dx'. \quad (46)$$

However, in general the intrinsic dynamics N and the activation function H are nonlinear and residual terms arise which are here notationally absorbed in Q and S. The intrinsic, sometimes also called endogenous, dynamics N of the neural mass action is defined by the temporal evolution of Ψ(x,t) in absence of all incoming signals including the connections to other neural masses. In the following we will discuss representative models from this line of approach and characterize the various entry points towards large scale network modeling.

We place particular emphasis on the functional effects that the variation of structural properties, such as local and global connectivity and time delays, implies.

Amari's Neural Field Model 1977

A classic paper on networks with no delay and symmetric and translationally invariant connection topologies is Amari's study of neural fields (Amari 1977). Amari discussed spatially and temporally continuous fields Ψ(x,t) with local fixed point dynamics as intrinsic dynamics. Then the field equations may be written as

$$\tau \frac{d\Psi\left(x,t\right)}{dt} = -\Psi\left(x,t\right) + \int\limits_{\Omega} h\left(x-x'\right) S\left(\Psi\left(x',t\right)\right) dx' + c + s(x,t)\ . \qquad (47)$$

where S is strongly nonlinear, typically the Heaviside function, and $h(x - x')$ is excitatory for proximate connections and inhibitory for greater distances (see Fig. 28 and 29). $s(x,t)$ denotes external input and c a constant resting potential and background activity.

In this type of scalar neural fields, oscillations are not possible, but locally excited regimes may exist and self-sustain with no input $s(x,t) = 0$, which is believed to be a candidate for the neuronal basis of working memory (Amit 1989). If input is provided, then the locally excited regions travel in the direction of increasing field value Ψ(x,t) until they get pinned at the stimulus location.

If several stimuli are provided, then the details of stimulus location and the presence of already excited local regions will determine the typically

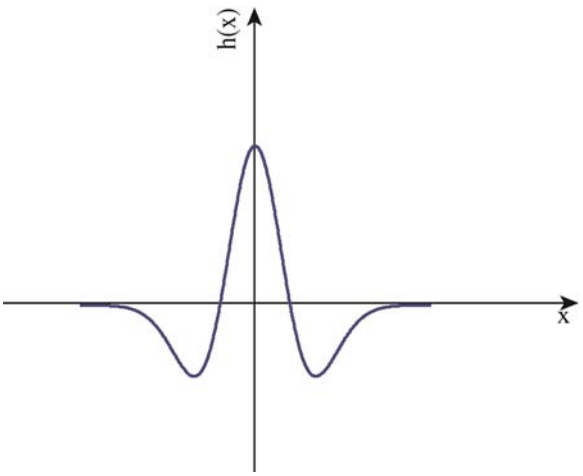

Fig. 28. Distribution function is plotted which captures local excitatory and lateral inhibitory connectivity

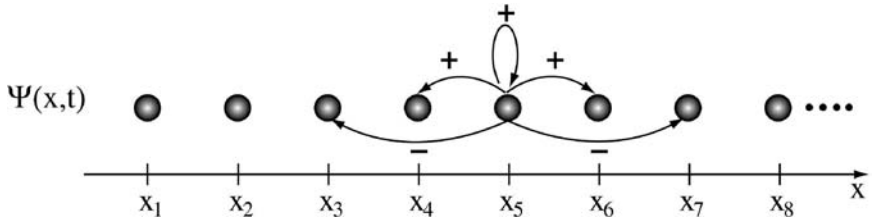

Fig. 29. The characteristic connectivity of an Amari field reflects local excitation and lateral inhibition

multi-stable final network dynamics. Characteristic examples are shown in Fig. 30(a), b and c.

In all cases, the final stationary network state will be a fixed point attractor. It was these properties, which attracted the attention of neural modelers who applied these fields to a variety of phenomena ranging from working memory (Amit 1989) to motor movement preparation (Erlhagen & Schöner 2002). If two or more layers are coupled (Amari 1977), then a more complex dynamics arises allowing for oscillatory and traveling wave phenomena.

The Neural Field Models of Wilson & Cowan (1972, 1973) and Nunez (1974)

Hugh Wilson & Jack Cowan (1972, 1973) and Paul Nunez (1974) independently considered twocomplementary approaches, of which each is based upon

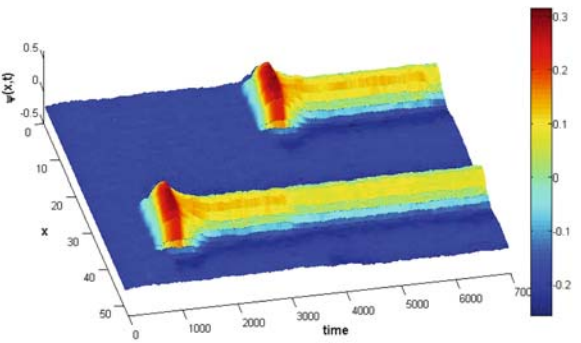

Fig. 30(a). The space-time diagram of an Amari field is shown. Initially the neural field is not excited, then a stimulus is introduced around 1000ms at location x = 35 (space is in arbitrary units). At stimulus offset around 1300ms, the neural field sustains its local excitation. At a later time point, another stimulus is introduced at x = 10 for 300ms. Here the neural field also persists after stimulus offset. Such persistent activity serves a s a simple model for working memory

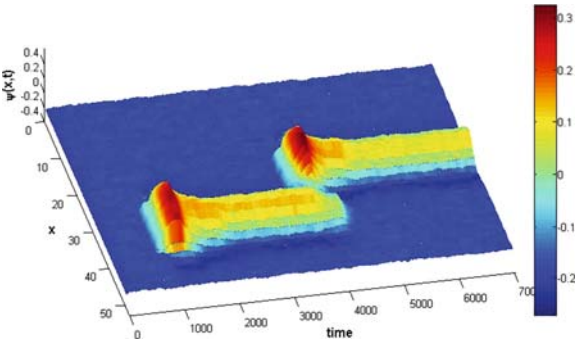

Fig. 30(b). The same situation is shown as in Figure 30a, only the second stimulus is provided closer in space, x = 25, to the first stimulus and annihilates the excitation at x = 35. The second local excitation persists unaltered

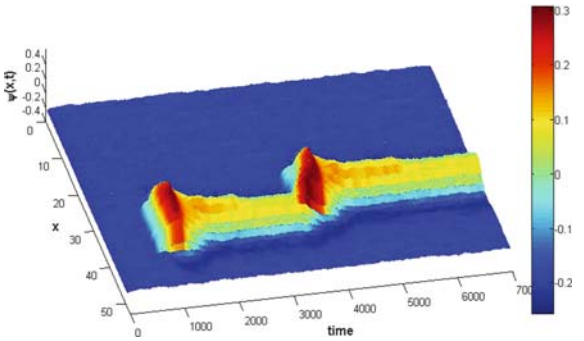

Fig. 30(c). The same situation is shown as in figure 30b, only the second stimulus is now provided even closer in space, x = 30, to the first stimulus than before. This time it does not annihilate the excitation at x = 35, on the contrary, both excitations move towards each other and merge into one excitation. In the figure, it appears that the excitation at x = 35 moves more than the other, which is true

two sets of locally coupled neural masses of inhibitory and excitatory neurons. Wilson & Cowan considered the firing rate as the neural mass action; Nunez considered synaptic action which is the proportion of active synapses at time t and linearly related to dendritic currents. The firing rate of neural masses has been referred to as pulses and the synaptic action as waves (Freeman 1975). Jirsa & Haken (1996, 1997) showed that both models are equivalent and can be transformed into each other using so-called pulse-wave and wave-pulse conversions, which are independently experimentally accessible (Freeman 1975). Both models consider time delays via propagation. Delays are absent in Amari's model and hence constrains the latter's applicability in a biologically realistic scenario to small patches of cortical tissue. Time delays are of increasing importance, the larger the scale of the network is.

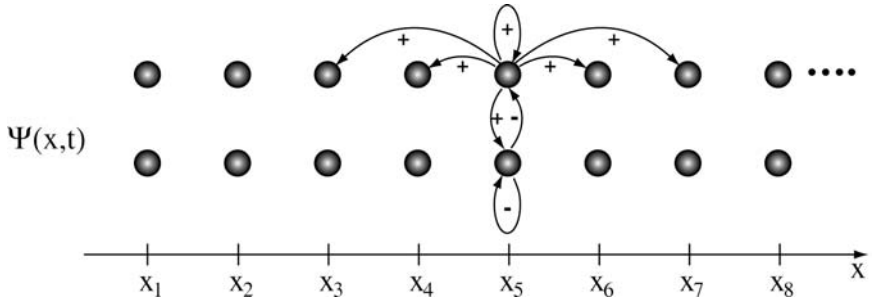

Fig. 31. The characteristic connectivity of Nunez's population approach reflects local and global excitation, as well as local inhibition

In Nunez's early work (1974), his focus was on identifying the dispersion relations of the linearized neural field dynamics given specific distributions of intracortical and corticocortical fiber systems. The intracortical fiber system is constrained to the gray matter and its axons make connections within a few millimeters; the corticocortical fiber system constitutes the white matter and connects areas across the entire cortex with axonal lengths of several centimeters in the human (Abeles 1991; Braitenberg & Schüz 1991), in some cases reaching lengths of up to 15 to 20 centimeters (Nunez 1995). The excitatory synaptic action Ψ_1(x,t) and inhibitory synaptic action Ψ_2(x,t) compose the neural mass action and define one excitatory and one inhibitory layer (see Fig. 31). The dynamics of the two-dimensional neural field is governed by the following equation

$$\frac{d\Psi\,(x,t)}{dt} = -\Psi\,(x,t) + s(x,t) + \int\limits_{\Omega}\int\limits_{0}^{\infty} h\,(x-x',v)\,S\left(\Psi\left(x,t-\frac{|x-x'|}{v}\right)\right)dvdx', \tag{48}$$

where $\Psi(x,t) = (\Psi_1(x,t),\ \Psi_2(x,t))$, s(x,t) is the input to the two layers, h(x−x',v) defines a matrix describing the distribution of axonal fibers, S is the sigmoid firing rate and Ω defines the spatial extent of the neural sheet. Due to the finite transmission speed v, there is a time delay $\frac{|x-x'|}{v}$ via propagation.

The connectivity function h(x−x',v) is a 2 by 2 matrix, since Ψ(x,t) is a 2-dimensional vector field, and considers both intracortical and corticocortical fibers collapsed into one distribution function. The synaptic influence is assumed to diminish in proportion to its density, in particular Nunez extrapolated h from mouse data (Nunez 1995) to assume an exponential form,

$$h(x) = \exp\left(-|x|/\sigma\right)/2\sigma, \tag{49}$$

as illustrated in Fig. 32, with the rate of drop-off captured by the parameter σ.

The inhibitory connectivity is of short range and the excitatory connectivity is of long-range since the latter is dominated by the corticocortical fiber

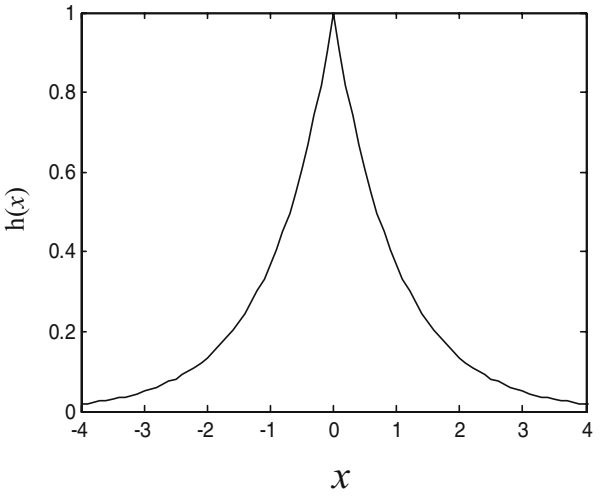

Fig. 32. Exponential coupling function

system. It is notable that Nunez's approach represents the first attempt to use structural information to constrain the neural field dynamics for the large scales observed in encephalographic measurements. His consideration of the corticocortical fiber system within the integral kernel of (49) has influenced much of the later research in the field of EEG and MEG (Jirsa & Haken 1996,1997; Wright and Liley 1996; Jirsa et al. 1998, 2002; Robinson et al. 1997, 2001; Steyn-Ross et al. 1999 ; Breakspear et al. 2006) and lead to the development of neural field dynamics for large scale systems.

Wilson & Cowan (1972) initially considered the interaction of two populations of excitatory and inhibitory nature characterized by their firing rates Ψ_1(t) and Ψ_2(t). An der Heiden (1980) showed nicely the connection between the local Wilson-Cowan population model (1972) and the McCulloch-Pitts model (1943). Later Wilson and Cowan (1973) extended their model to two layers of coupled neural fields Ψ_1(x,t) and Ψ_2(x,t) (see Fig. 33) obeying the following equation

$$\frac{d\Psi\left(x,t\right)}{dt} = -\Psi\left(x,t\right) + S\left(\int\limits_{\Omega} h\left(x-x'\right)\Psi\left(x,t-\frac{\left|x-x'\right|}{v}\right)dx' + s(x,t)\right), \tag{50}$$

where we use the same notation as in the Nunez model. Various dynamic phenomena were found as a function of the connectivity h including steady network states, standing and traveling waves. An emphasis was placed on the spatial localization of activations, which functionally necessitated the constraint that inhibitory connections are of longer range than excitatory interactions. Such is in analogy to Amari's model and is anatomically reflected in the longer axons of inhibitory interneurons. This constraint, however, requires

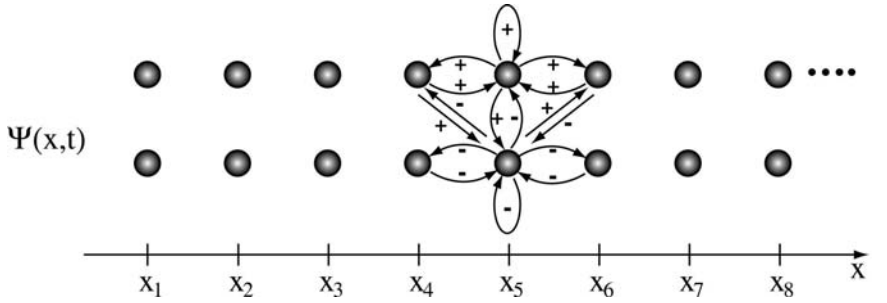

Fig. 33. The characteristic connectivity of Wilson & Cowan's coupled population approach reflects local excitation and inhibition with various degrees of laterality

the axons not to leave the gray matter and clearly limits the application of these neural fields to local area networks.

The Neural Field Model of Jirsa & Haken (1996) and Wave Equations

Based on first principles using pulse-wave and wave-pulse conversions, Jirsa & Haken (1996, 1997) developed a neural field approach (see for early accounts of neural field theories Griffith 1963, 1965) targeted specifically towards large scale phenomena as observed in EEG, MEG. Initially based on two locally coupled neural masses of excitatory and inhibitory neurons, the action of the inhibitory neural mass is absorbed into an effective excitatory neural mass action $\Psi(x,t)$. This reduction is possible under the assumption that the intrisic dynamics of the neural mass is negligible and relaxes instantly to its steady state, i.e. the neural mass action displays a fixed point dynamics. Then the network dynamics will exclusively be determined by the connectivity and its time delays and captured by an equation equivalent to (48), but with a scalar connectivity function $h(x-x')$ (see Fig. 34). As in the Nunez model, the connectivity includes local intracortical connections and global corticocortical projections. As a first approximation, $h(x-x')$ is assumed to be translationally invariant and follows an exponential decay as plotted in Fig. 32. Under these

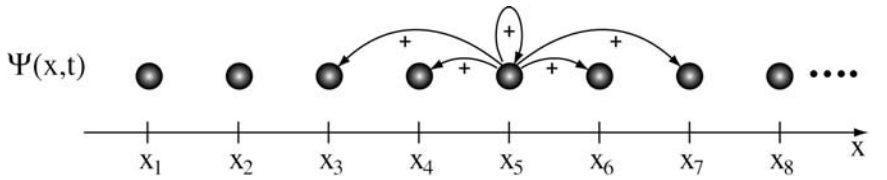

Fig. 34. The characteristic connectivity of the Jirsa-Haken wave equation emphasizes excitatory long range connectivity after elimination of the local inhibitory effects. The latter are captured in an effective neural mass action $\Psi(x,t)$

conditions, Jirsa & Haken showed that the integro-differential (48) is equivalent to the following partial differential equation in one physical dimension:

$$\frac{\partial^2 \Psi(x,t)}{\partial^2 t} + 2\omega_0 \frac{\partial \Psi(x,t)}{\partial t} - v^2 \frac{\partial^2 \Psi(x,t)}{\partial^2 x} + \omega_0^2 \psi(x,t) = \omega_0(\omega_0 + \frac{\partial}{\partial t}) S(\Psi(x,t)) \tag{51}$$

where $\omega_0 = v/\sigma$, v is the transmission speed along myelinated axons and σ the mean fiber length. Early accounts of wave phenomena in EEG and their discussion in the context of wave equations can be found in (Nunez 1995).

The Jirsa-Haken wave equation (51) approximates various connectivity functions of large scale networks in the limit for long waves, or, in other words, large scale activity patterns. If the slope of the sigmoid function S increases beyond a threshold, then the rest state becomes unstable and undamped wave propagation occurs. Below the threshold damped wave propagation exists. Steven Coombes and colleagues (2003) discuss the effects of connectivity strengths which do not decrease with increasing distance, but rather remain constant within a finite regime. In this case, it is not sufficient to describe the spatiotemporal dynamics by a local partial differential equation as in (51), but non-local delayed terms arise (see Coombes 2005 for a review). Wright and colleagues introduced much physiological detail and were able to address issues of rhythm generation (Wright & Liley 1996), as well as clinical aspects such as hysteresis phenomena in anesthesia (Steyn-Ross et al. 1999). Robinson and colleagues introduced expressions for the corticothalamic loop into the Jirsa-Haken equation (see next section) and included dendritic dynamics while implementing detailed physiologically realistic parameter ranges (Robinson 1997, 2001). Frank and colleagues developed a Fokker-Planck approach to the Jirsa-Haken equation which captures the time evolution of the stochastic properties of the neural fields (Frank et al. 1999, 2000). Applications to encephalograpic data can be found in (Jirsa and Haken 1997; Jirsa et al. 1998, 2002; Fuchs et al. 2000; Liley et al. 2002; Jirsa 2004b; Robinson et al. 2004, 2005; Breakspear et al. 2006).

The Inclusion of the Thalamocortical Loop into Neural Fields (Robinson 2001)

In 1997 Robinson et al. presented an equivalent derivation of the Jirsa-Haken equation considering effects of dendritic dynamics and added the important extension of the thalamocortical loop in 2001 (see Fig. 35). The inclusion of the thalamocortical interactions proved to be crucial to reproduce the essential spectral properties observed in scalp topographies. Robinson and colleagues preserve the neural field as a vector field $\Psi(\mathrm{x},\mathrm{t}) = (\Psi_1(\mathrm{x},\mathrm{t}),\ \Psi_2(\mathrm{x},\mathrm{t}))$ of excitatory and inhibitory neural masses and write the following equations

$$\begin{aligned} \frac{\partial^2 \Psi(\mathbf{x},t)}{\partial^2 t} + 2\omega_0 \frac{\partial \Psi(\mathbf{x},t)}{\partial t} - v^2 \frac{\partial^2 \Psi(\mathbf{x},t)}{\partial^2 x} + {\omega_0}^2 \psi(\mathbf{x},t) \\ = {\omega_0}^2 \rho(\Psi(\mathbf{x},t), \Psi_{th}(t - \boldsymbol{\tau}/2)) \end{aligned} \tag{52}$$

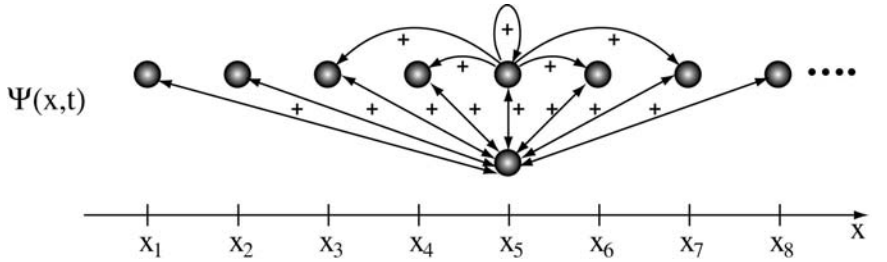

Fig. 35. Robinson et al. (2001) capture corticothalamic effects contributing to neural field dynamics. The effect of excitatory and inhibitory influences is collapsed into the upper row

for the dynamics of the neural field. The critical step is that the sigmoid function $\rho(\Psi(\mathbf{x}, t))$ does not only depend on the neural fields Ψ_1(x,t), Ψ_2(x,t), but also receives time–delayed thalamic input $\Psi_{\mathrm{th}}(\mathrm{t} - \tau/2)$.

The thalamic action $\Psi_{\mathrm{th}}(\mathrm{t})$ is governed by the following differential equation

$$\frac{\partial^2 \Psi_{th}(t)}{\partial^2 t} + (a+b)\frac{\partial \Psi_{th}(t)}{\partial t} + ab\Psi_{th}(t) = \mathrm{input}(\Psi(x, t - \tau/2)) \qquad (53)$$

where the cortical input to the thalamus also undergoes a delay $\tau/2$ via propagation resulting in a effective delay τ of the total corticothalamic loop. Computer simulations of equations (52) and (53) provide representative EEG power spectra as shown in Fig. 36.

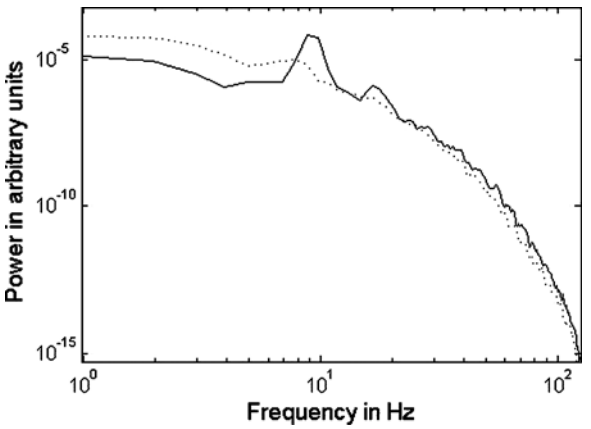

Fig. 36. Power spectra from the Robinson model of corticothalamic activity in eyes closed (solid) and eyes open (dashed) resting states. The increase of low frequencies in the eyes open condition reflects increased corticocortical gain, whereas the increased alpha (10 Hz) peak in the eyes closed condition reflects increased corticothalamic gain

Extensions and Limitations of Large Scale Models

Large scale systems are characterized by an anatomical connectivity with massively parallel and serial, hierarchical structures, as well as time delays due to signal transmission. Such architecture produces an interareal connection topology, which is patchy as observed by Braitenberg & Schüz (2001) and results in a heterogeneous connectivity. Yet it has been approximated in various attempts by a homogeneous connectivity with a larger extension (see Fig. 37). The approach uses a larger mean path length and hence effectively mixes functionally the intracortical and corticocortical fiber systems. Research of this kind has successfully reproduced various large scale characteristics of activity including the dispersive properties of the cortex (Nunez 1995) or global EEG power spectra (Robinson 2001); it also shows promise in situations of highly symmetric functional connectivity (Jirsa et al. 1997, 1998; Fuchs et al. 2000). However, to this date, it has not been shown rigorously under what conditions the homogeneous approximation holds.

Mallot and colleagues (1989, 1996) discussed in a series of papers a conceptual framework in which, rather than just mean fields, local networks communicate across distances. These local networks have an intrinsic fixed point dynamics, but exchange information via time-delayed pathways. Mallot and colleagues applied this approach to examples of the thalamocortical loop (Mallot et al. 1996) and for the geniculate-striate pathway of the visual system (Mallot et al. 1989). Similarly, discretely coupled local networks incorporate time delays in the connecting pathways and absorb all local dynamics within a set of coupled neural masses (Freeman 1975, 1992; David & Frison 2003). Jirsa & Kelso (2000) studied the neural field dynamics of the Jirsa-Haken equation in which a heterogeneous pathway is included (Fig. 38). Such a two-point pathway connects the neural masses at locations X_2 and X_8 which are embedded into a continuous sheet with local connections only. This

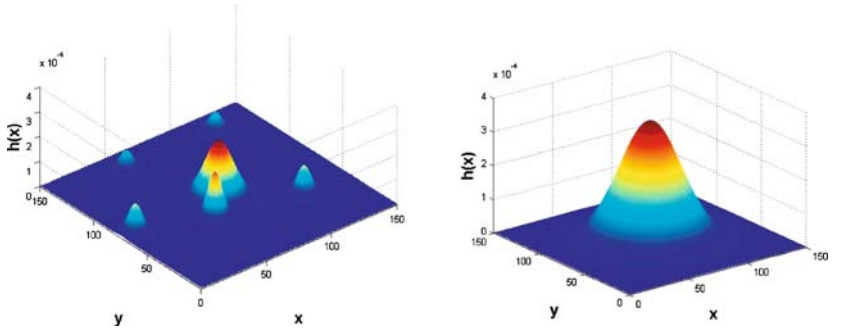

Fig. 37. Left: Neural connectivity has local intracortical symmetric components (homogeneous) and patchy corticocortical components (heterogeneous). Right: Approximation of the real local and global connectivity by a symmetric connectivity function with an average path length

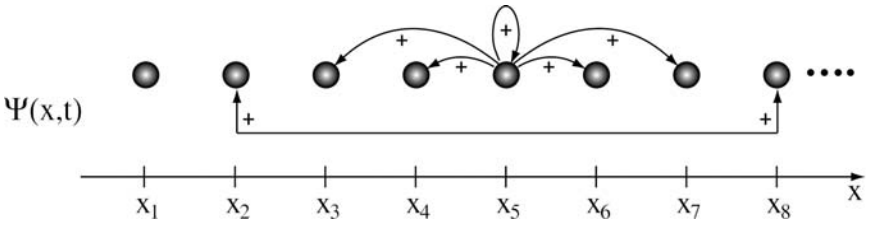

Fig. 38. Realistic connectivities are characterized by translationally invariant local connections and translationally variant global connections. The basic model for the study of the interplay of local and global interactions is the embedded two-point connection in a locally connected neural network as shown in the figure

connectivity identifies the basic toy model for the study of local and global interactions. The change in the connection topology destabilizes the initial stationary dynamics and the system undergoes a transition to a new stationary state via a Hopf bifurcation. Detailed bifurcation diagrams are given in (Jirsa & Kelso 2000) in which the spatiotemporal reorganization is characterized as a function of the length of the two point connection.

Minor changes in the location of the terminals or the system parameters, such as the homogeneous or heterogeneous transmission speeds, may result in qualitatively different global neural field dynamics. As an example, in Fig. 39 a stimulus is introduced in the neighborhood of a terminal of a two-point

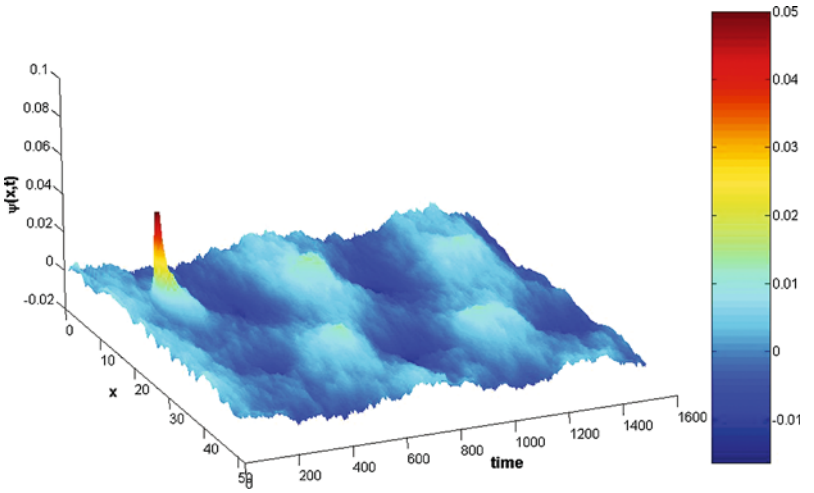

Fig. 39. A neural field following Jirsa and Haken (1996) with an embedded two-point connection at x=10 and x=40 is established. In the neighborhood of x=10, a brief stimulus excites the neural sheet locally and the neural field reorganizes globally in a large scale transient wave which damps out after a sufficiently long time (not shown here)

connection (based at x=10 and x=40), then the excitation of the neural field travels through the continuous sheet, but also transmits a signal via the heterogeneous pathway. A transient wave dynamics is observed on the global system scale and damps out after a sufficiently long enough time. With no heterogeneous connection, only a local excitation at x=10 would have been observed. Similarly, with no heterogeneous connection and with two stimuli at terminal sites x=10 and x=40, only two local excitations would have been observed, but no large scale organization as observed in Fig. 39.

5 Conclusion

The neurosciences have historically leaned strongly towards empiricism – a tradition which continues today. However, mathematical formalisms of dynamical phenomena have provided extraordinary explanatory and unifying insights in the physical sciences. The emerging advances in computational neurosciences, particularly with respect to brain connectivity, suggest that they will also come to play an important role in the brain sciences. The cross-fertilization of dynamical systems theory (see also the Chapters by Campbell, Horowitz & Husain and Stephan & Friston), graph theory (Sporns & Tononi), basic physics (Ferree & Nunez), and methodological advances in neuroimaging (Darvas & Leahy, Fuchs) will hopefully underpin advances which do not merely reduce problems in neuroscience to problems already solved in other fields, but instead allow those properties of the brain that are unique to inform novel and specific discoveries. We see this blending of universality and specificity as absolutely crucial. Too much of the former will yield simplifications that lose what is required of a system in order to look (and function) like a brain. Conversely, too much specific detail yields volumes of descriptive data that adds little to our understanding of the underlying principles of brain function.

In this chapter, we have overviewed developments in the field of dynamical neural modeling across several scales of magnitude – from the microscopic conductance models of bifurcating neurons, (briefly) through systems of coupled chaotic oscillators at the mesoscopic scale to models of large scale neural networks whose behavior generates the electroencephalographic and neuroimaging data that is acquired non-invasively from human subjects. Evidence of computationally significant processes has been documented in data sets from across this spectrum of scales – i.e. from the single cell to the whole brain. An open and important question then is the relationship between activity at different temporal and spatial scales (Churchland and Sejnowski 1992). A possible answer could be that the macroscopic dynamics is an epiphenomenon – that is, a summed output of dynamics that can only truly be modeled at the neuronal level. However, this approach cannot be reconciled with the successes of large-scale models, which engage the brain at macroscopic scales only, to provide descriptive explanations of neuroscience data. That is, as discussed in

Sect. 4 of the present chapter, a mean field reduction of the present state of the system is able to predict its future states. This suggests that synchronizing processes are able to enslave many of the (small scale) degrees of freedom into dynamical structures at larger scales whose behavior is then – to some degree – determined by the state of the system *at that scale*. Whilst the large scale processes that are sustained by such processes inevitably influence the dynamics of the small scale units, it also remains possible that small scale events – such as critical sensory inputs – are able to rapidly influence the behavior of the system as a whole.

Whilst such considerations preclude a purely reductionist approach, an adequate explanatory framework remains elusive. The situation may be analogous to a heated magnet that it is close to the Curie temperature (above which it loses the ability to be magnetized): The magnetic fields *are purely* an outcome of the dipoles of spinning electrons. Yet the spinning electrons are also strongly influenced by the larger-scale magnetic fields. Below the Curie temperature, the fields are sufficiently strong to overcome stochastic fluctuations of individual spin directions. Above the Curie temperature the emergent fields are insufficient in strength to enslave the electron dipoles and the metal cannot hold a macroscopic field. However, at the Curie temperature, there is just a sufficient degree of coherence at any given scale to overcome the stochastic fluctuations at the next smaller scale. However, fluctuations at a small scale are able to transiently cascade to larger scales, a phenomena known as *criticality* and exhibit scale free fluctuations. Or perhaps even more attractive are the *spin glass* systems where – in addition to these processes – there exist disordered structures embedded in the system which preclude a perfectly ordered system even at low temperatures. Many of such spatiotemporal pattern formation phenomena and their underlying mechanisms have been understood in the framework of *Synergetics*, a field pioneered by Hermann Haken (1983, 1999).

Whilst such arguments have an attractive appeal, we should bear in mind our own warning that the brain is *not* just another complex physical system – such as a heated metal – even one with embedded impurities! There exist additional complexities that are surely important to brain function. One such critical difference is that there do exist structures across spatial and temporal scales prior to the emergence of dynamically driven scale-free (and scale-specific) fluctuations. Is it possible that the interaction between scale-specific processes across a hierarchy of scales is somehow optimal? Fusi *et al.* (2005) have shown how a hierarchy of synaptic processes – each with characteristic time scales – can interact in order to optimize memory retention (upgrading new memories) and storage (maintaining selected memory for long periods of time). Breakspear & Stam (2005) modeled the interaction between scale-free dynamics and multiscale spatial architectures by defining dynamical systems on different wavelet subspaces, and with cross-scale coupling between subspaces. This would potentially allow for a recursive relationship between small and large-scale dynamics.

Such observations hopefully reflect the challenge of fusing the universal with the specific as an emerging frontier in neuroscience research.

Acknowledgements

The authors wish to acknowledge helpful comments by SA Knock, PL Nunez, PA Robinson and E Tognoli and funding by ATIP (CNRS), Brain NRG JSMF22002082, NH&MRC, Australia and ARC Australia.

References

Abeles M (1991) Corticonics. Cambridge University Press

Abeles M, Bergman H, Margalit E, Vaadia E (1993) Spatiotemporal firing patterns in the frontal cortex of behaving monkeys. J. Neurophysiol.70, 1629–1638

Abbott LF, van Vreeswijk C (1993) Asynchronous states in a network of pulse-coupled oscillators. Phys. Rev. E 48, 1482–1490

Abraham RH, Shaw CD (1988) Dynamics – The Geometry of Behavior. Part Four: Bifurcation Behavior. Addison-Wesley: Redwood City.

Afraimovich V, Verichev N, Rabinovich M (1986) Stochastic synchronization of oscillation in dissipative systems. Radiophysics and Quantum Electronics 29, 795–801.

Amari S (1977) Dynamics of pattern formation in lateral-inhibition type neural fields. Biol. Cybern. 27, 77–87

Amit DJ (1989) Modelling Brain Function. New York, Cambridge University Press

Amit DJ, Brunel N (1997) Model of global spontaneous activity and local structured activity during delay periods in the cerebral cortex. Cerebral Cortex 7, 237–252

An der Heiden U (1980). Analysis of neural networks. In Lecture Notes in Biomathematics (S Levin, ed), volume 35. Springer-Verlag, New York

Arbib M, Érdi P (2000) Structure, Function, and Dynamics: An Integrated Approach to Neural Organization. Behavioral and Brain Sciences 23, 513–571

Ashwin P, Buescu, J, Stewart, I (1996) From attractor to chaotic saddle: A tale of transverse stability. Nonlinearity, 9: 703–737.

Ashwin P, Terry J (2000) On riddling and weak attractors. Physica D, 142, 87–100.

Baker GL, Gollub JP (1990) Chaotic Dynamics: An Introduction. Cambridge University Press

Barana Gy, Gröbler T, Érdi P (1988) Statistical model of the hippocampal CA3 region I. The single-cell module: bursting model of the pyramidal cell. Biol. Cybern. 79, 301–308

Beggs JM, Klukas J, Chen W (2007) Connectivity and dynamics in local cortical networks. This Volume.

Beurle RL (1956) Properties of a mass of cells capable of regenerating pulses. Philos. Trans. Soc. London Ser. A240, 55–94

Braitenberg V, Schüz A (1991) Anatomy of the cortex. Statistics and geometry. Springer, Berlin Heidelberg New York

Breakspear M, Terry J, Friston KJ (2003) Modulation of excitatory synaptic coupling facilitates synchronization and complex dynamics in a nonlinear model of neuronal dynamics Network: Computation in Neural Systems 14, 703–732
Breakspear M (2004) "Dynamic" connectivity in neural systems: Theoretical and empirical considerations. Neuroinformatics 4,1–23.
Breakspear M, Stam KJ (2005) Dynamics of a neural system with a multiscale architecture. Phil. Trans. R. Soc. B 360, 1051–1074.
Breakspear M, Roberts JA, Terry JR, Rodrigues S, Robinson PA (2006) A unifying explanation of generalized seizures via the bifurcation analysis of a dynamical brain model. Cerebral Cortex, doi:10.1093/cercor/bhj072.
Bressler SL (1990) The gamma wave: a cortical information carrier? Trends in Neuroscience 13(5), 161–162
Bressler SL (1995) Large-scale cortical networks and cognition. Brain Res. Rev. 20, 288–304
Bressler SL (2002) Understanding cognition through large-scale cortical networks. Curr. Dir. Psych. Sci. 11, 58–61
Bressler SL (2003) Cortical coordination dynamics and the disorganization syndrome in schizophrenia. Neuropsychpharmacology 28, 535–539
Bressler SL, Kelso JAS (2001) Cortical coordination dynamics and cognition. Trends in Cog. Sci. 5, 26–36
Bressler SL, Tognoli E (2006) International Journal of Psychophysiology (in press)
Bressler SL, McIntosh AR (2007) The role of neural context in large-scale neurocognitive network operations. This Volume.
Brunel N, Hakim V (1999) Fast global oscillations in networks of integrate-and-fire neurons with low firing rates. Neural Comput. 11, 1621–1671
Bullmore ET, Rabe-Hesketh S, Morris RG, Williams SC, Gregory L, Gray JA, Brammer MJ (1996) Functional magnetic resonance image analysis of a large-scale neurocognitive network. Neuroimage 4, 16–33
Campbell SA (2007) Time Delays in Neural Systems. This Volume.
Cessac B, Samuelides M (2006) From Neuron to Neural Network Dynamics. To appear in Dynamical Neural Network. Models and Applications to Neural Computation. Springer Berlin Heidelberg New York
Chu PH, Milton JG, Cowan JD (1994) Connectivity and the dynamics of integrate-and-fire neural networks. Int. J. Bifur. Chaos 4, 237–217
Churchland P, Sejnowski TJ (1992) The Compuational Brain. MIT Press. New York.
Collet P, Eckmann J (1980) Iterated maps on the interval as dynamical systems, Birkhauser.
Coombes S, Lord GJ, Owen MR (2003) Waves and bumps in neuronal networks with axo-dendritic synaptic interactions. Physica D, 178, 219–241
Coombes S (2005) Waves, bumps, and patterns in neural field theories, Biological Cybernetics 93, 91–108
Crick F, Koch C ((1990) Towards a neurobiological theory of consciousness. Seminars in the Neurosciences 2, 263–275
Cvitanovic P (1984) Universality in chaos. Adam Hilger: Bristol.
Dayan P, Abbott LF (2001) Theoretical Neuroscience. MIT Press Cambridge, Massachusetts
De Monte S, d'Ovidio F, Mosekilde E (2003) Coherent regimes of globally coupled dynamical systems. Phys. Rev. Let. 90, 054102

Dhamala M, Jirsa VK, Ding M (2004) Transitions to synchrony in coupled bursting neurons. Phys. Rev. Lett. 92: 028101.
Eckmann J, Ruelle D (1985) Ergodic theory of chaos and strange attractors. Reviews of Modern Physics, 57: 617–656
Erlhagen W, Schöner G (2002) Dynamic field theory of movement preparation.. Psychological Review 109, 545–572
Ermentrout B (1998) Neural networks as spatio-temporal pattern-forming systems. Rep. Prog. Phys. 61: 353–430.
Feigenbaum MJ (1978) Quantitative universality for a class of nonlinear transformations. J. Stat. Phys., 19: 25–52.
Ferree TC, Nunez PL (2007) Primer on electroencephalography for functional connectivity. This volume
FitzHugh R (1961) Impulses and physiological states in theoretical models of nerve membrane. Biophys. J. 1, 445–466
Frank TD, Daffertshofer A, Beek PJ, Haken H (1999) Impacts of noise on a field theoretical model of the human brain. Physica D, 127, 233–249
Frank TD, Daffertshofer A, Peper CE, Beek PJ, Haken H (2000) Towards a comprehensive theory of brain activity: coupled oscillator systems under external forces. Physica D, 144, 62–86
Freeman WJ (1975) Mass action in the nervous system. Academic Press New York
Freeman WJ, Skarda CA (1985) Spatial EEG patterns, nonlinear dynamics and perception: the neo-Sheringtonian view. Brain Res Rev10, 147–175
Freeman WJ (1987) Simulation of chaotic EEG patterns with a dynamic model of the olfactory system. Biological Cybernetics, 56, 139–150
Freeman WJ (1992) Tutorial on neurobiology: From single neurons to brain chaos. Inter. Journ. Bif. Chaos 2, 451–482
Fuchs A, Jirsa VK, Kelso JA (2000) Theory of the relation between human brain activity (MEG) and hand movements. Neuroimage 11(5), 359–369
Fujisaka H, Yamada T (1983) Stability theory of synchronized motion in coupled-oscillator system. Progress in Theoretical Physics, 69, 32–47.
Fusi S, Drew PJ, Abbott LF (2005). Cascade models of synaptically stored memories. Neuron. 45, 599–611.
Gardiner CW (2004) Handbook of Stochastic Methods. Springer Berlin Heidelberg New York
Gerstner W (2000) Population Dynamics of Spiking Neurons: Fast Transients, Asynchronous States, and Locking. Neural Computation 12, 43–89
Gerstner W, Kistler WM (2002) Spiking neuron models: Single neurons, populations, plasticity. Cambridge University Press
Gray CM, Singer W (1989) Stimulus-specific neuronal oscillations in orientation columns of cat visual cortex. Proc. Nat. Acad. Sci. 86, 1698–1702
Grebogi C, Ott E, Yorke JA (1982) Chaotic atractors in crisis. Phys. Rev. Lett. 48: 1507–1510.
Griffith JS (1963) A field theory of neural nets: I. Derivation of field equations. Bull. Math. Biophys. 25, 111–120
Griffith JS (1965) A field theory of neural nets: II. Properties of the field equations. Bull. Math. Biophys. 27, 187–195
Gröbler T, Barna Gy, Érdi P (1988) Statistical model of the hippocampal CA3 region II. The population frame work: model of rhythmic activity in the CA3 slice. Biol. Cybern. 79, 309–321

Grossberg S (1988) Nonlinear Neural Networks: Principles, Mechanisms, and Architectures. Neural Networks 1, 17–61

Guckenheimer, J. (1987) Limit sets of S-unimodal maps with zero entropy, Communications in Mathematical Physics, 110: 655–659.

Guevara MG (2003). Dynamics of excitable cells. In: Nonlinear Dynamics in Physiology and Medicine (A Beuter, L Glass, MC Mackey and MS Titcombe, eds). Springer-Verlag, New York, pp. 87–121.

Haken H (1983) Synergetics. An introduction. 3rd edition. Springer Berlin, Heidelberg, New York

Haken H (1999) Information and Self-Organization. 2nd edition. Springer Berlin, Heidelberg, New York

Hindmarsh JL, Rose RM (1984) A model of neuronal bursting using three coupled first order differential equations. Proc. R. Soc. London, Ser. B 221, 87

Hodgkin AL, Huxley AF (1952) A Quantitative Description of Membrane Current and its Application to Conduction and Excitation in Nerve/Journal of Physiology, 117: 500–544

Hopfield JJ (1982) Neural networks and physical systems with emergent collective computational abilities. Proc. Nat. Acad. Sci. 79, 2554–2558

Hopfield JJ (1984) Neurons with graded response have collective computational properties like those of two-state neurons. Proc. Nat. Acad. Sci. 81, 3088–3092

Horwitz B, Friston KJ, Taylor JG (2000) Neural modeling and functional brain imaging: an overview. Neural Networks 13, 829–846

Izhikevich E (2005) Dynamical systems in neuroscience: The geometry of excitability and bursting. MIT Press.

Jirsa VK, Haken H (1996) Field theory of electromagnetic brain activity. Physical Review Letters, 77: 960–963.

Jirsa VK, Haken H (1997) A derivation of a macroscopic field theory of the brain from the quasi-microscopic neural dynamics. Physica D 99: 503–526.

Jirsa VK, Fuchs A, Kelso JAS (1998) Connecting cortical and behavioral dynamics: bimanual coordination. Neural Computation 10, 2019–2045

Jirsa VK, Kelso JAS. (2000) Spatiotemporal pattern formation in continuous systems with heterogeneous connection topologies. Phys. Rev. E 62, 6, 8462–8465

Jirsa VK, Jantzen KJ, Fuchs A, Kelso JAS (2002) Spatiotemporal forward solution of the EEG and MEG using network modeling. IEEE Transactions on Medical Imaging, 21, 5, 493–504

Jirsa VK (2004) Connectivity and dynamics of neural information processing. Neuroinformatics 2 (2), 183–204

Jirsa VK (2004b) Information processing in brain and behavior displayed in large-scale scalp topographies such as EEG and MEG. Inter. J. Bif. Chaos 14(2), 679–692

Kaneko K (1997) Dominance of Milnor attractors and noise-induced selection in a multiattractor system. Physical Review Letters, 78: 2736–2739

Kiss T, Érdi P (2002) Mesoscopic Neurodynamics. BioSystems 64, 119–126

Koch C (1999) Biophysics of Computation. Information processing in single neurons. Oxford University Press

Larter R, Speelman B and Worth R M (1999) A coupled ordinary differential equation lattice model for the simulation of epileptic seizures. *Chaos*, **9**: 795–804.

Liley DTJ, Cadusch PJ, Dafilis MP (2002) A spatially continuous mean field theory of electrocortical activity. Network-Computation in Neural Systems, 13, 67–113.

Lopes da Silva FH, Hoeks A, Smits H, Zetterberg LH (1974) Model of brain rhythmic activity: the alpha-rhythm of the thalamus. Kybernetik 15,27–37

Lopes da Silva FH, Blanes W, Kalitzin S, Parra J, Suffczynski P, Velis DN (2003) Dynamical diseases of brain systems: different routes to epileptic seizures Trans. Biomed. Eng. 50: 540–548.

Lorenz, E (1963) Deterministic nonperiodic flow. Journal of Atmospheric Science, 20: 130–141.

Maistrenko Y, Maistrenko V, Popovich A, Mosekilde E (1998) Transverse instability and riddled basins in a system of two coupled logistic maps. Physical Review E, 57: 2713–2724.

Mallot HA, Brittinger R (1989) Towards a network theory of cortical areas. In: Cotteril RMJ. (ed) Models of brain function. Cambridge University Press, 175–189

Mallot HA, Giannakopoulos F (1996) population networks: a large-scale framework for modelling cortical neural networks. Biological Cybernatics 75, 441–452

McCormick DA, Bal T (1997) Sleep and Arousal: Thalamocortical mechanisms. Ann. Rev. Neuroscience, 20: 185–215

McCulloch WS, Pitts W (1943) A logical calculus of the ideas immanent in nervous activity. Bull. Math. Biophys. 5:115–33.

McIntosh AR (2000) Towards a network theory of cognition. Neural Netw. 13, 861–876

Mesulam MM (1998) From sensation to cognition. Ann. Neurol. 28, 597–613

Milton JG (1996) Dynamics of small neural populations. American Mathematical Society

Milton JG, Chkhenkeli SA, Towle VL (2007) Brain Connectivity and the Spread of Epileptic Seizures. This volume.

Milnor J (1985) On the concept of attractor. Communications in Mathematical Physics, 99: 177–195.

Morris C, Lecar H (1981) Voltage oscillations in the barnacle giant muscle fiber. Biophysics J., 35: 193–213

Mountcastle VB (1978) An organizing principle for cerebral function: the unit module and the distributed system. In: Edelman GM, Mountcastle VB (Eds) The Mindful Brain. MIT Press, Cambridge MA

Mountcastle VB (1998) Perceptual Neuroscience: the cerebral cortex. Harvard University Press, Cambridge MA

Nagumo J, Arimoto S, Yoshizawa S (1962) An active pulse transmission line
simulating nerve axon. Proc IRE. 50: 2061–2070.

Nunez PL (1974) The brain wave equation: a model for the EEG. Mathematical Biosciences 21: 279–297.

Nunez PL (1995) Neocortical dynamics and human EEG rhythms, Oxford University Press

Nykamp DQ, Tranchina D (2001) A population density approach that facilitates large-scale modeling of neural networks: Extension to slow inhibitory synapses. Neural Computation 13, 511–546

Nykamp DQ, Tranchina D (2000) A population density approach that facilitates large-scale modeling of neural networks: analysis and an application to orientation tuning. Journal of Computational Neuroscience 8, 19–50

Ratliff F, Knight BW, Graham N (1969) On tuning and amplification by lateral inhibition. PNAS 3: 733–740.

Robinson PA, Rennie CJ, Wright JJ (1997) Propagation and stability of waves of electrical activity in the cerebral cortex. Physical Review E, 56: 826–840.

Robinson PA, Rennie CJ, Wright JJ, Bahramali H, Gordon E, Rowe DL (2001) Prediction of electroencephalographic spectra from neurophysiology. Physical Review E 63, 021903

Robinson PA, Rennie CJ, Rowe DL (2002) Dynamics of large-scale brain activity in normal arousal states and epileptic seizures. Physical Review E 65, 041924.

Robinson PA, Rennie CJ, Rowe DL, O'Connor SC (2004) Hum Brain Mapp 25, 53–72

Robinson PA, Rennie CJ, Rowe DL, O'Connor SC, Gordon E (2005) Phil. Trans. Roy. Soc. Ser. B 360, 1043

Rodriguez, S, Terry JR, Breakspear M (2006) On the genesis of spike-wave activity in a mean-field model of human corticothalamic dynamics. Physics Letters A 355, 352–357

Rosenblatt F (1958) The perceptron: a probabilistic model for information storage and organization in the brain, Psychol. Rev. 65: 386–408.

Rulkov N, Sushchik M, Tsimring L, Abarbenel H (1995) Generalized synchronization of chaos in unidirectionally coupled chaotic systems. *Physical Review E*, **51**: 980–994.

Sejnowski TJ, Rosenberg CR (1987) Parallel networks that learn to pronounce English. Complex Systems, 1: 145–168.

Smalheiser NR (2000) Walter Pitts. Perspectives in Biology and Medicine. 43: 217–226.

Sporns O (2003) Complex Neural Dynamics. In: Coordination Dynamics: Issues and Trends. Jirsa VK & Kelso JAS (eds.) Springer Berlin

Sporns O, Tononi G (2002) Classes of Network connectivity and dynamics. Complexity 7, 28–38

Sporns O, Tononi G (2007) Structural determinants of functional brain dynamics. This Volume.

Strogatz SH (1994) Nonlinear dynamics and Chaos. Addison-Wesley: Reading, MA.

Steyn-Ross ML, Steyn-Ross DA, Sleigh JW, Liley DTJ (1999) Theoretical electroencephalogram stationary spectrum for a white-noise-driven cortex: Evidence for a general anesthetic-induced phase transition. Phys. Rev. E 60, 7299–7311

Szentagothai J (1975) The 'module-concept' in cerebral cortex architecture. Brain Res. 95, 476–496

Tagamets MA, Horwitz B (1998) Integrating electrophysiological and anatomical experimental data to create a large-scale model that simulates a delayed match-to-sample human brain imaging study. Cereb. Cortex 8, 310–320

Treisman A (1996) The binding problem. Curr. Pin. Neurobiol. 6, 171–178

van Rotterdam A, Lopes da Silva FH, van den Ende J, Viergever MA, Hermans AJ (1982) A model of the spatio- temporal characteristics of the alpha rhythm. Bulletin of Mathematical Biology. 44: 283–305.

Valdes PA, Jimenez JC, Riera J, Biscay R, Ozaki T (1999) Nonlinear EEG analysis on a neural mass model. Biol. Cybern. 81, 415–424

Ventriglia F (1974) Kinetic approach to neural system. Bull. Math. Biol. 36, 535–544

Ventriglia F (1978) Propagation of excitation in a model of neural system. Biol. Cybern. 30, 75–79

Von Stein A, Rappelsberger P, Sarnthein J, Petsche H (1999) Synchronization between temporal and parietal cortex during multimodal object processing in man. Cereb. Cortex 9, 137–150

Wilson HR (1973) Cooperative phenomena in a homogenous cortical tissue model. In: Haken H. (ed.) Synergetics – Cooperative Phenomena in Multi-compartment Systems. B. G. Teubner, Stuttgart

Wilson HR and Cowan JD (1972) Excitatory and inhibitory interactions in localized populations of model neurons. Biophys. J. 12, 1–23.

Wilson HR, Cowan JD (1973) A mathematical theory of the functional dynamics of cortical and thalamic nervous tissue. Kybernetic 13, 55–80

Wright JJ, Liley DTJ (1996) Dynamics of the brain at global and microscopic scales: Neural networks and the EEG. Behav. Brain. Sci. 19, 285